Physics at the Tevatron

Rick Field[1]

Department of Physics, University of Florida, Gainesville, Florida, 32611, USA

Abstract: The theme of the XXXIV International Meeting on Fundamental Physics held in El Escorial, Spain on April 2-7, 2006 was "From HERA and the TEVATRON to the LHC". This is a summary of the four lectures I presented on "Physics at the Tevatron". Heavy quark production and the production of photons, bosons, and jets at the Tevatron are discussed. Also, a detailed study at the "underlying event" at CDF is presented together with a discussion of PYTHIA 6.2 tunes. A look back at the "old days" of Feynman-Field collider phenomenology is included.

I. INTRODUCTION

The Tevatron, located at Fermilab near Chicago, Illinois, USA, collides protons with antiprotons at a center-of-mass energy of 1.96 TeV. As shown in Fig. 1.1, CDF and DØ are the two collider detector experiments at Fermilab. The Tevatron is currently the highest energy collider in the world and lately it has been performing very well. The delivered integrated luminosity per week is about 25 pb^{-1} and both CDF and DØ have more that 1.2 fb^{-1} of data collected on tape (see Fig. 1.2). At the Tevatron we are beginning to measure cross-sections that are at the 1 pb level or smaller, which is very exciting. Many important new physics results were presented at the winter conferences earlier this year. I cannot show all the interesting Tevatron results in just four lectures. I will show a few of the many important Tevatron measurements and I will show more from CDF than DØ simply because I am a member of CDF and therefore I am more familiar with the CDF analyses.
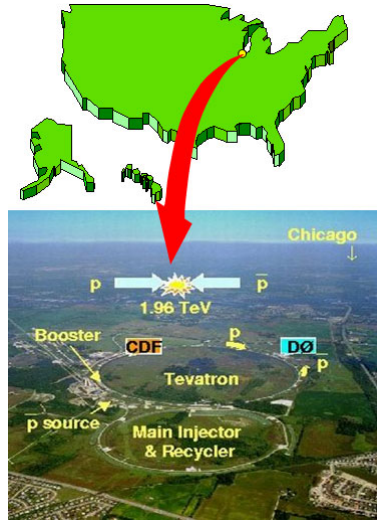

Fig. 1.1. Arial photograph of the Tevatron, located at Fermilab near Chicago, Illinois, USA which collides protons with antiprotons at a center-of-mass energy of 1.96 TeV. CDF and DØ are the two collider detector experiments at Fermilab.

I will begin in Section II by taking a look back at the "old days" of Feynman-Field collider phenomenology. I think it is important for students to see how far we have come in our understanding of hadron-hadron collisions since 1973. In Section III I will discuss heavy quark production at the Tevatron and Section IV will be devoted to photons and bosons. Finally, in Section IV I will present a detailed study at the "underlying event" at CDF and discuss Run 2 PYTHIA 6.2 tunes.
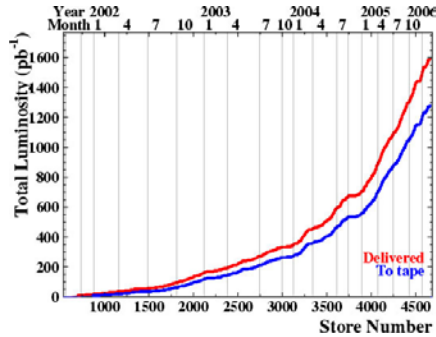

Fig. 1.2. Shows the total integrated luminosity delivered (and collected to tape by CDF) at the Tevatron in Run 2.

II. FROM FEYNMAN-FIELD TO THE TEVATRON

When I arrived at CALTECH in 1973 it was already clear from SLAC deep inelastic scattering experiments that the proton was a composite particle made up of tiny hard pieces which were referred to as "partons". Also, there was mounting evidence that at least some of the partons were quarks. We knew that only about 50% of the protons momentum was carried by the quarks, but I do not think we knew that the other 50% was carried by point-like massless gluons. The ISR at CERN was studying proton-proton collisions at a center-of-mass energy of 53 GeV and Fermilab was colliding 200 GeV protons on fixed targets (*i.e.* $W = \sqrt{s} = 19.2$ GeV).

When two protons of equal and opposite momentum collide at high energy most of the time they simply fall apart producing a collection of hadrons moving along the direction of the two incoming protons and all of the outgoing particles have small transverse momenta relative to the beam direction (~ 300 MeV/c). However, it was noticed that occasionally a high transverse momentum, p_T, hadron (pion or kaon) would be produced. This did not happen often but it happened more often then one would expect if the proton was a "soft" object. In those days high transverse momentum meant anything with $p_T > 2$ GeV/c and the highest transverse momentums observed were only around 7 GeV/c!

In about 1974 Feynman and I were wondering about where these high transverse momentum hadrons came from. We did not believe that a pion traveling in the direction of one of the incoming protons could "turn the corner" and come out at high transverse momentum without falling apart into its constituent quarks. We believed that the high p_T particles came from a hard 2-to-2 scattering of the quarks within the incoming protons. The two outgoing high transverse momentum quarks would then fragment into pions and kaons some of which would have high p_T. At that time we did not know how to calculate the quark-quark elastic scattering differential cross section. The theory of Quantum Chromodynamics (QCD) was just beginning to be understood

and the perturbative 2-to-2 parton-parton differential cross sections had not yet been calculated. People were just beginning to realize that QCD was an asymptotically free
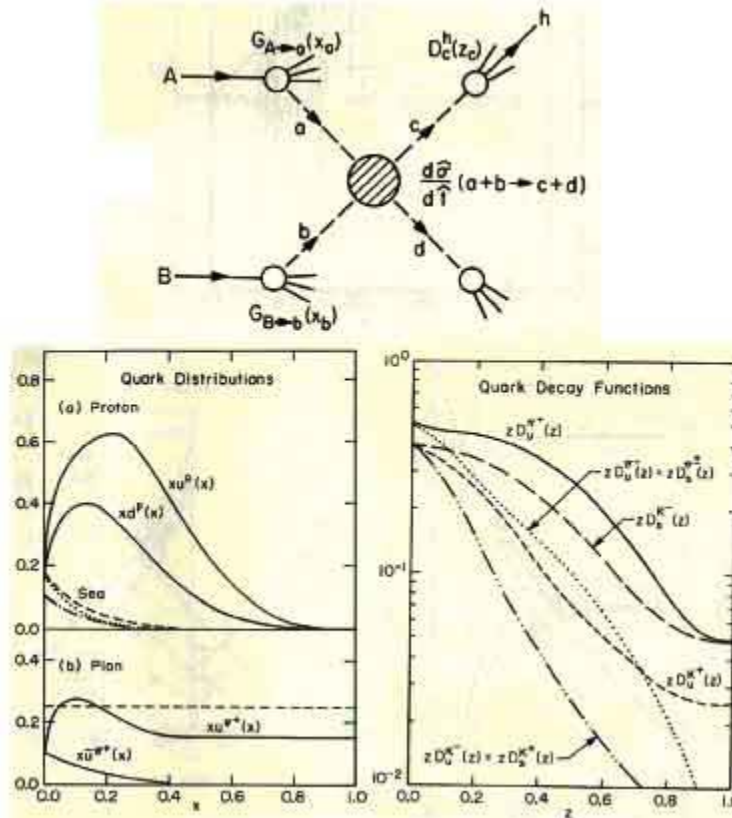

Fig. 2.1. Illustration of the Feynman-Field quark-quark elastic scattering "black-box" model for hadron-hadron collisions from FF1 (1977). (*top*) The model assumed that high p_T particles arise from direct hard collisions between constituent quarks in the incoming particles, which fragment or cascade down into several hadrons. (*bottom left*) The quark distribution functions were determined by fitting the SLAC deep inelastic scattering data. (*bottom right*) The quark fragmentation functions were determined by fitting e^+e^- data and the 2-to-2 quark-quark elastic scattering cross section, $d\sigma/dt$, was determined by fitting the data (*i.e.* "black-box").

theory which allows perturbation theory to be applied at high p_T. Because we did not yet understand how to calculate anything, in the first Feynman-Field paper (FF1) [1] which we completed in 1975, but did not publish until 1977 we concocted the "quark-quark elastic scattering black-box" model which is illustrated in Fig. 2.1. We fit the SLAC deep inelastic scattering data to determine the probability of finding a quark of flavor f within a proton carrying a fraction, x, of the protons momentum, $G_{p \to f}(x)$. In addition, we fit e+e- data to determine the probability that a hadron, h, carrying fractional momentum, z, of an outgoing quark of flavor, f, is contained among the fragmentation products, $F_{f \to h}(z)$. The proton structure functions (we called them quark distribution functions) and quark fragmentation functions (we called them quark decay functions) were assumed to scale (*i.e.* were a function only of the fractional momentum x or z). We took the quark-quark elastic scattering differential cross section to be a "black-box" and determined it by fitting the data.

I wrote the first draft of the Feynman-Field papers and Feynman would come in and give me sentences or paragraphs that he would like to include in the paper. The following is a Feynman quote from FF1: *"The model we shall choose is not a popular one, so that we will not duplicate too much of the work of others who are similarly*

analyzing various models (e.g. constituent interchange model, multiperipheral models, etc.). We shall assume that the high p_T particles arise from direct hard collisions between constituent quarks in the incoming particles, which fragment or cascade down into several hadrons."
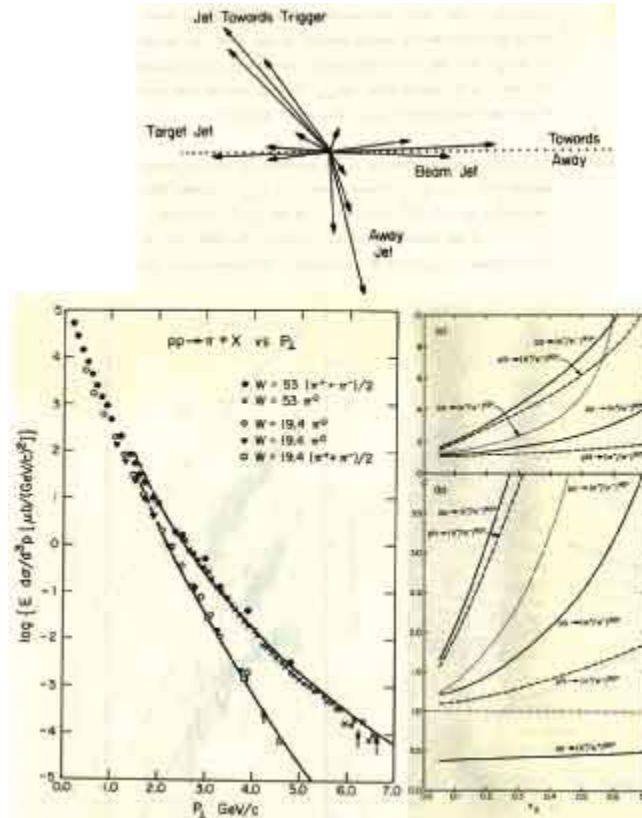

Fig. 2.2. (top) Shows the topology predicted by the Feynman-Field quark-quark elastic scattering "black-box" model for hadron-hadron from FF1 (1977) in which there is a "toward" side "jet" (*i.e.* collection of hadrons moving roughly in the same direction) and an "away" jet, together with the beam and target jet (*i.e.* the "beam-beam" remnants). Also shows the predictions of the model for the inclusive meson cross section at 19.4 GeV and 53 GeV (bottom left) and for the high pT particle rations at 53 GeV (a) and 19.4 GeV (b).

The "black-box" model was naïve, however, it convinced us we were on the right track. As illustrated in Fig. 2.2, we adjusted the quark-quark elastic differential cross section to fit the experimentally measured high p_T meson cross section at W = 19.4 GeV and then predicted it correctly at W = 53 GeV. The rise in the cross section, of course, comes from the parton distribution function. We were amazed that we were able to use electron-proton and e+e- data to predict something about hadron-hadron collisions. The model also predicted the topology in high p_T hadron-hadron collisions that we are all familiar with today in which there is a "toward" side "jet" (*i.e.* collection of hadrons moving roughly in the same direction) and an "away" jet, together with the "beam-beam remnants" (we called them the beam and target jet). We studied this topology in more detail in FFF1 [2]. The "beam-beam remnants" are part of the "underlying event" in hadron-hadron collisions which I will discuss in Section V.

In FF1 we were able to predict particle ratios at high p_T. Actually, the reason we waited two years to publish the paper is that the model predicted the π^+/π^- ratio would increase at large p_T in proton-proton collisions and Feynman wanted to see some

evidence of this before we published the paper. In July 1976 Feynman was at a meeting in Les Houches where he learned from Jim Cronin that the University of Chicago group did see the increase we expected in an experiment at Fermilab. The x_T = $2p_T/W$ values at the ISR were too small to see much of an effect. I received a telegram which Feynman sent from Les Houches which stated: *"Saw Cronin – Am now convinced were right track – Quick write – Feynman"*.

We knew we were on the right track, but as you can see in retrospect there were many things we did not understand. For one, we thought the pion structure function went to a constant at high x and similarly we thought the quark fragmentation function to a pion went to a constant at large z. Of course, we all know now that there can be a constant term in these functions, but they are the so-called "higher twist" terms and fall off as a power of Q^2. Also, the "black-box" model did not include gluons. At that time we did not realize the gluon is a "hard" point-like parton just like the quark. We thought of it more like "glue".
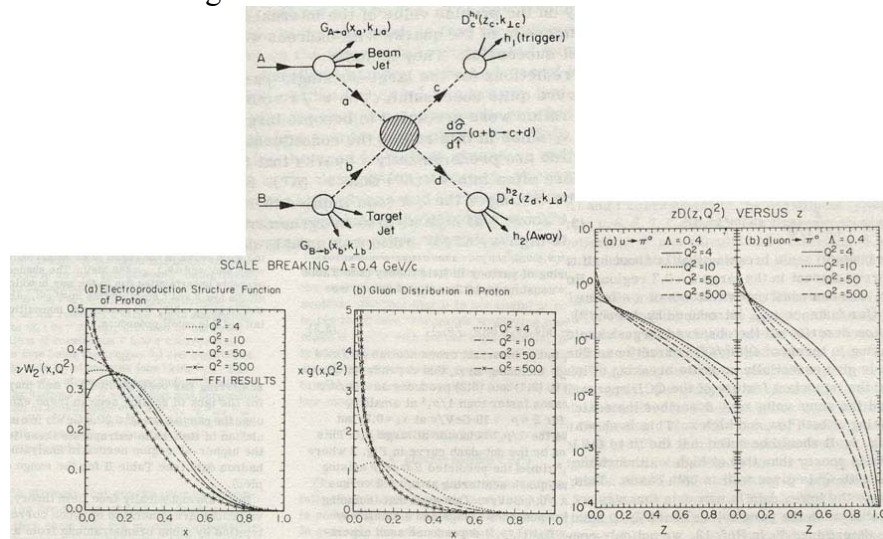

Fig. 2.3. Illustration of the QCD model for hadron-hadron collisions from FFF2 (1978). (*top*) The model assumed that high p_T particles arise from direct hard collisions between constituent quarks and gluons in the incoming particles, which fragment into "jets" of hadrons. (*bottom left*) The quark distribution functions were determined by fitting the SLAC deep inelastic scattering data at Q^2 = 4 GeV and determined at other values of Q^2 using QCD perturbation theory (*bottom right*) The quark fragmentation functions were determined by fitting e^+e^- data and the 2-to-2 quark-quark elastic scattering cross section, ds/dt, was determined from the data (i.e. "black-box").

The "black-box" model lasted less than a year. Things were happening fast. Even before the paper was published we were learning more about QCD. Once we realized it is an asymptotically free theory and that we could use perturbation theory to calculate high p_T phenomena we did everything over again, but this time using QCD as illustrated in Fig. 2.3. The parton distribution functions (PDF's) and the fragmentation functions now depended on the scale of the hard scattering (*i.e.* Q^2). Gluons were now included and all of the seven parton-parton scattering differential cross sections were calculated by perturbation theory. Fig. 2.4 shows some of the predictions of the QCD approach with Λ = 400 MeV from FFF2 (1978) [3,4]. We realized that the "jet" cross section was much larger than the cross section to produce a single charged hadron at the same p_T. We did not know if they would ever build a collider with a center-of-mass energy of 1 TeV, but as can be seen in Fig. 2.4, in 1978 we predicted the "jet" cross section at W = 1 TeV. However, our transverse

momentum scale only extended out to 30 GeV/c!   The prediction at p_T = 30 GeV/c is shown on the recent inclusive jet cross section measured at CDF.   Due to the resolution of the CDF calorimeter it is difficult to measure the jet cross section below 60 GeV/c.   What we thought in 1978 was a high p_T jet is too low of a p_T to be measured at the Tevatron!   Fig. 2.5 shows a "lego" plot of a high p_T di-jet event measured in the CDF calorimeter. Comparing Fig. 2.2 with the CDF jet data shows the wonderful journey from 7 GeV/c π^0's to 600 GeV/c jets! The CDF high p_T jet events are a bit "cleaner" than we would have thought back in 1978. This is because at that time we were using a QCD scale Λ of around 400 MeV and today we know that it is much smaller (around ~200 MeV). Small Λ means a small QCD coupling α_s and hence less initial and final state gluon radiation, resulting in "cleaner" di-jet events. The following is a Feynman quote from FFF2: *"At the time of this writing, there is still no sharp quantitative test of QCD. An important test will come in connection with the phenomena of high p_T discussed here."*
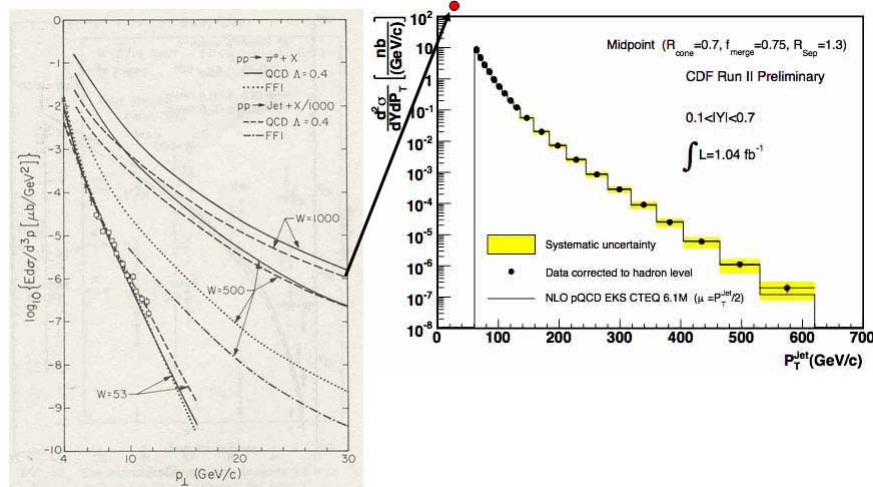

Fig. 2.4. (*left*) Predictions of the QCD model for meson and "jet" production hadron-hadron collisions from FFF2 (1978). (*right*) CDF Run 2 data on the inclusive "jet" cross section at 1.96 TeV with an integrated luminosity of 1 fb-1.
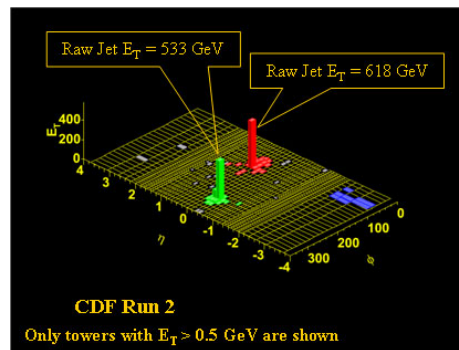

Fig. 2.5. CDF Run 2 di-jet event at 1.96 TeV with (raw) jet transverse energies of 403 GeV and 322 GeV observed in July 2002.

The calculations in FF1, FFF1, and FFF2 were done analytically by convoluting (*i.e.* integrating) over the parton distribution functions, fragmentation functions, and the parton cross sections. We wanted to be able to simulate on an event-by-event bases hadron-hadron collisions (and e^+e^- annihilations) using Monte-Carlo techniques, but to do so would require a model for the way the outgoing quarks and gluons fragment into hadrons. In FF2 (1978) [5] Feynman and I proposed a simple model for

parameterizing the properties of quark jets. The model assumes that quark jets can be analyzed on the basis of a recursive principle illustrated in Fig. 2.6. Our "chain decay" ansatz assumed that, if the rank 1 meson carries away momentum ξ, from a quark of flavor "a" and momentum P_0, the remaining cascade starts with a quark of flavor "b" and momentum $P_1 = P_0 - \xi$, and the remaining hadrons are described in precisely the same way as the hadrons which came from a jet originated by a quark of flavor "b" with momentum P_1. There is one generating function, $f(y)$, which gives the probability that the rank 1 meson leaves fractional momentum y to the remaining cascade. The generating function was determined by fitting the e^+e^- data. Additional parameters were included to handle the flavor dependence of the fragmentation functions. We let β_u be the probability that the new quark-antiquark pair is a $u\bar{u}$ pair, and β_d be the probability that it is a $d\bar{d}$ pair, etc.. We later generalized the model to include gluon jets. The following is a Feynman quote from FF2: *"The predictions of the model are reasonable enough physically that we expect it may be close enough to reality to be useful in designing future experiments and to serve as a reasonable approximation to compare to data. We do not think of the model as a sound physical theory"*.
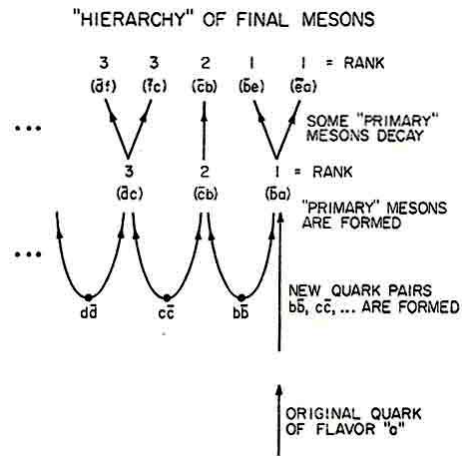

Fig. 2.6. Illustration of the hierarchy of mesons formed when a quark of flavor "a" fragments into hadrons from FF2 (1978). The initial quark of flavor "a" combines with an antiquark from a produced quark-antiquark pair, "bbbar", forming the meson for rank 1. The resulting quark of flavor "b" then combines with an antiquark from another produced quark-antiquark pair forming the meson of rank 2 and so on. These "primary" mesons are then allowed to decay into "secondary" mesons.

The Feynman-Field jet model (FF fragmentation) was, of course, a naive scaling model and QCD certainly modifies the approach. Nevertheless, it was very easy to implement the model using Monte-Carlo techniques and it allowed us, for the first time, to simulate hadron-hadron collisions (and e^+e^- annihilations) on an event-by-event basis. In 1978 we constructed a QCD Monte-Carlo event generator for hadron-hadron collisions (and e^+e^- annihilations) and began making predictions for experiment.

As shown in Fig. 2.7, quarks radiate gluons producing a "parton shower" which can be computed using perturbative QCD down to some small scale Q_0 at which time things become non-perturbative and hadrons are formed. It only makes sense to use the FF fragmentation model if one stops the parton shower at a rather high scale, say around 5 GeV. One needs another fragmentation approach if you want to generate the parton shower down to a smaller scale. With many partons of low momentum you

cannot independently fragment each one of them using the FF model. In FW1 (1983) [6] my first graduate student, Steven Wolfram, and I proposed a "cluster" fragmentation model which was more closely connected to perturbative QCD than the FF fragmentation model. Here one evolves the parton shower down to a rather low scale, follow the color flow, and forms low invariant mass color singlet clusters which are then allowed to decay into hadrons using two-body phase space. Our QCD Monte-Carlo event generator had a switch which allowed us to run either of the two approaches. We could stop the parton shower evolution at a high scale and employ FF fragmentation to parameterize the rest of the hadronization process or we could evolve the parton-shower down to a small Q^2 and employ the simple two-body phase space decay model (*i.e.* FW fragmentation).
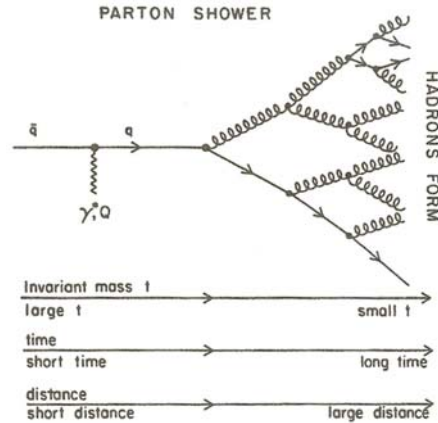
Fig. 2.7. Illustration of a "parton shower" in which a quark initially produced at a scale Q radiates gluons which in turn radiate additional gluons and quark-antiquark pairs. As time increases the shower progresses to larger distances from the point where in initial quark was produced and the invariant masses, t, of the partons decrease from a maximum of Q^2 to some small scale Q_0 where hadrons are formed.

Feynman warned me not to release our QCD Monte-Carlo event generator to the experimenters to use. He felt that it would become a "black box" to them and that they would take the predictions too seriously without understanding the subtitles involved in constructing the generator. Later Frank Paige constructed ISAJET [7] which uses FF fragmentation and Bryan Webber constructed HERWIG [8] which uses an improved version of FW fragmentation. PYTHIA [9] uses a "string fragmentation" model invented in 1983 by the Lund group [10]. PYTHIA, HERWIG, and ISAJET employ different fragmentation models.
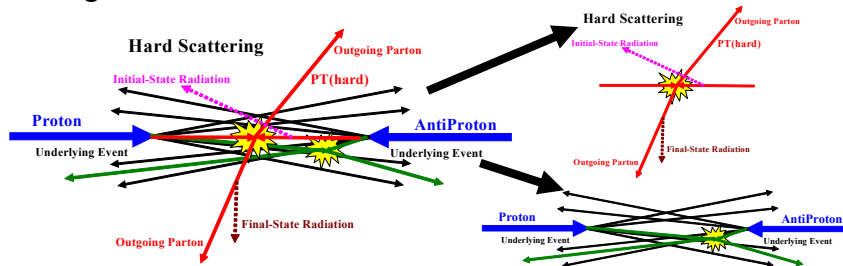

Fig. 2.8. Illustration of the way QCD Monte-Carlo models simulate a proton-antiproton collision in which a "hard" 2-to-2 parton scattering with transverse momentum, P_T(hard), has occurred. The "hard scattering" component of the event consists of particles that result from the hadronization of the two outgoing partons (*i.e.* the initial two "jets") plus the particles that arise from initial and final state radiation (*i.e.* multijets). The "underlying event" consists of particles that arise from the "beam-beam remnants" and from multiple parton interactions.

Fig. 2.8 illustrates the way the modern QCD Monte-Carlo models simulate a proton-antiproton collision in which a "hard" 2-to-2 parton scattering with transverse momentum, P_T(hard), has occurred. The "hard scattering" component of the event consists of particles that result from the hadronization of the two outgoing partons (*i.e.* the initial two "jets") plus the particles that arise from initial and final state radiation (*i.e.* multijets). The "underlying event" consists of particles that arise from the "beam-beam remnants" and from multiple parton interactions (MPI). Of course, in a given event it is not possible to uniquely determine the origin of the outgoing particles and whatever observable one chooses to study inevitably receives contributions from both the hard component and the underlying event. I will discuss the tuning of the QCD Monte-Carlo model generators to fit the CDF "underlying event" data in Section V.
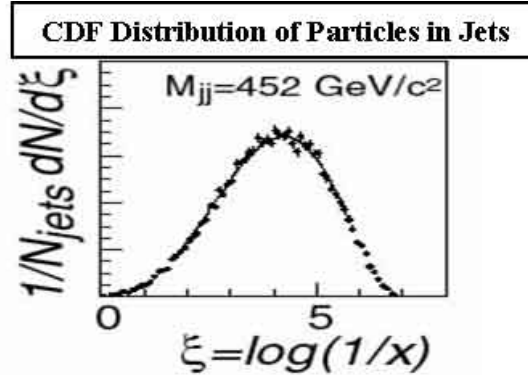
Fig. 2.9. CDF data on the distribution of charged particles within the two jets for di-jet events at 1.8 TeV with an invariant mass of 452 GeV/c^2. The plot shows the number of charged particles with $\xi = \log(1/x)$ and $x = p_{chg}/E_{jet}$ (points). The data are compared with the MLLA distribution of partons evolved down to a scale $Q_0 = 230$ MeV (curve) assuming a constant value of $N_{chg}/N_{parton} = 0.56$ to convert from partons to charged hadrons.

In the MLLA approach [11] the parton shower is evolved down to a very small scale (~ 200 MeV) and there is no fragmentation into hadrons. Instead one assumes that the outgoing hadrons follow the distribution of partons (*i.e.* local parton hadron duality [12]). Fig. 2.9 shows CDF data on the distribution of charged particles within the two jets for di-jet events at 1.8 TeV. The curve is the MLLA distribution of partons evolved down to a scale $Q_0 = 230$ MeV multiplied by a constant value of $N_{chg}/N_{parton} = 0.56$ to convert from partons to charged hadrons. It appears that if you evolve the parton shower down a very low scale you do not have to have a fragmentation model! This amazes me since many of the charged hadrons come from the decay of resonances and hence one is not seeing the "primary" meson distribution. Nevertheless it seems to work.

Experimentally we measure "jets" at the detector level (*i.e.* calorimeter level) by observing the energy in each calorimeter cell as illustrated in Fig. 2.10. Of course the "jet" cross section depends on ones choice of jet algorithm. Each jet algorithm is a different observable and comparing the results of different jet algorithm teaches us about QCD. Of course, what is measured in the calorimeter must be corrected for detector efficiency which is done by comparing the QCD Monte-Carlo models at the particle (*i.e.* generator level) with the result after detector simulation. I believe that experimenters should publish what they measure (*i.e.* observables at the particle level with the "underlying event"). However, to determine the parton distribution functions accurately one must calculate at next-to-leading order (NLO). At present there is no QCD Monte-Carlo generator at NLO (*i.e.* MC@NLO) for the production of light

quarks and gluons in hadron-hadron collisions. At present, the NLO parton level does not have fragmentation or an "underlying event". There are three approaches for comparing data corrected to the particle level (*i.e.* hadron level) with parton level calculations.
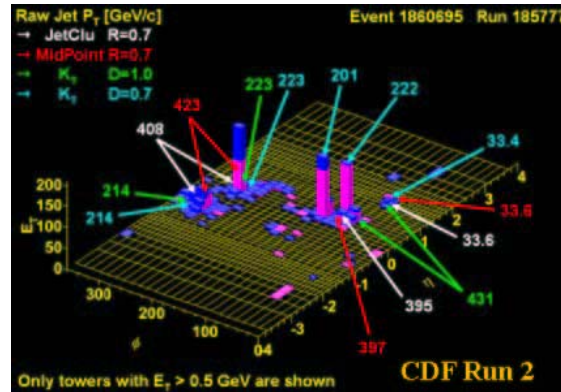

Fig. 2.10. Shows the transverse energy of calorimeter towers with $E_T > 0.5$ GeV for an event in the CDF detector. The MidPoint algorithm combines the two clusters into one "jet" with $p_T = 423$ GeV/c while the K_T algorithm (D = 0.7) finds two "jets" with $p_T = 223$ GeV/c and 214 GeV/c.

The first approach is to neglect the difference and to compare the hadron level data directly with the parton level calculation. Fig. 2.11 shows the inclusive jet cross section using the MidPoint algorithm (R = 0.7, f_{merge} = 0.5) for two rapidity bins as measured by DØ. DØ compares the experimentally measured hadron level prediction directly with the NLO parton level theory curves and assumes that the parton level to hadron level corrections are small for jets above 50 GeV. The agreement between the parton-level theory prediction and the measured hadron-level is quite good.
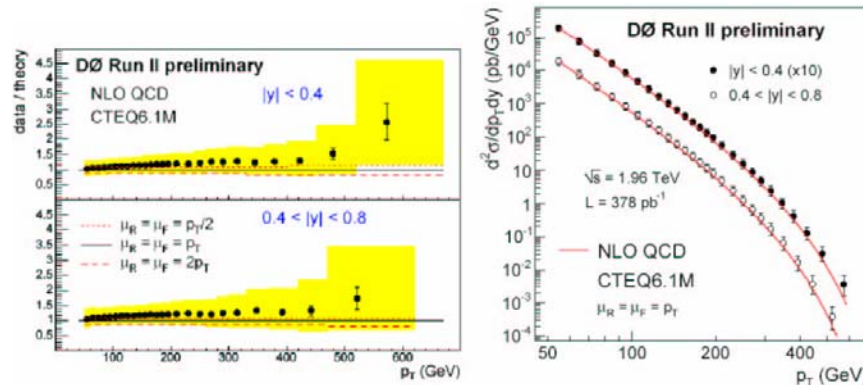
Fig. 2.11. The DØ Run 2 inclusive jet cross section using the MidPoint algorithm (R = 0.7, f_{merge} = 0.50) compared with parton-level NLO QCD. The hadron-level data are compared directly with the parton-level NLO QCD.

Another approach for comparing what is measured at the particle level in the detector with the NLO parton level theory is to use the QCD Monte-Carlo models and try to extrapolate the data to the parton level. This requires removing the "underlying event" and correcting for fragmentation effects. Fig. 2.12 shows the inclusive jet cross section using the MidPoint algorithm (R = 0.7, f_{merge} = 0.75) in the central region as measured by CDF compared with the parton level NLO QCD prediction, where the data have been extrapolated (*i.e.* corrected) to the parton level. Fig. 2.12 shows that the hadron level to parton level correction factors are significant for p_T(jet) < 300

GeV/c (they come mostly from the "underlying event"). Nonetheless, the agreement between the theory and data is very good.
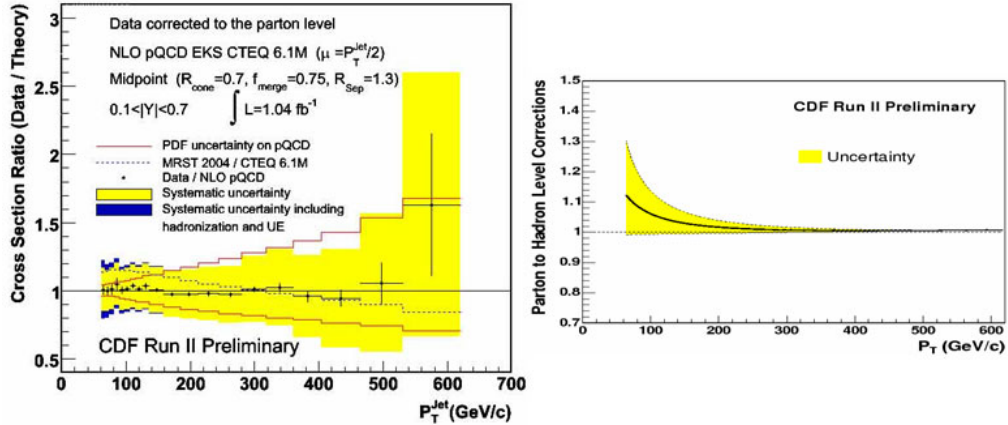

Fig. 2.12. The CDF Run 2 inclusive jet cross section using the MidPoint algorithm (R = 0.7, f_{merge} = 0.75) compared with parton-level NLO QCD (*left*). The data have been extrapolated (*i.e.* corrected) to the parton level using the parton to hadron correction factor (*right*). The hadron-level data are multiplied by the reciprocal of this factor.
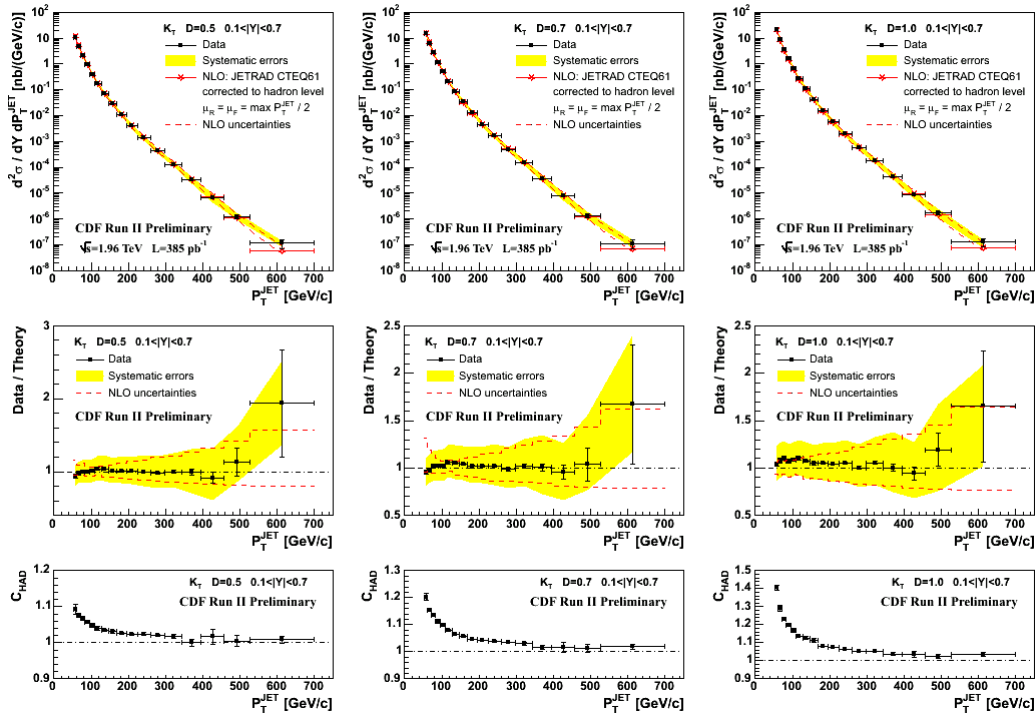

Fig. 2.13. The CDF Run 2 inclusive jet cross section using the K_T algorithm with D = 0.5, 0.7, and 1.0. The data are at the particle level (with an "underlying event") and the NLO parton level (CTEQ61M) has been corrected for fragmentation effects and for the "underlying event" (with correction factors C_{HAD}).

A third approach for comparing what is measured at the particle level in the detector with the NLO parton level theory is to use the QCD Monte-Carlo models to correct the NLO parton level theory by adding in the effects of fragmentation and the "underlying event". Even though the ratio of data to theory is identical in both approaches, I prefer this approach. It is much better to correct the theory to the hadron level (with an "underlying event") than it is to extrapolate a perfectly good

experimental observable to something that is not observable (*i.e.* parton level). Fig. 4 shows the CDF Run 2 inclusive jet cross section using the K_T algorithm. Here the data are at the particle level (*i.e.* hadron level) and the NLO parton level theory has been corrected to the particle level. As for the MidPoint algorithm, the parton level to hadron level corrections are significant for p_T(jet) < 300 GeV/c (coming mostly from the "underlying event"). The agreement between the theory and data is good.

The MidPoint cone jet algorithm has several undesirable features. An arbitrary procedure must be implemented to split and merge overlapping calorimeter cones. In addition an ad-hoc parameter, R_{sep}, is required to accommodate the differences between jets defined at the at the parton and detector level. Furthermore, cone algorithms implemented with "seeds", like the MidPoint algorithm, are not infrared safe at the parton level in perturbative QCD at NNLO, and exhibit sensitivity to soft radiation.

The K_T algorithm [13] is the preferred jet algorithm in e^+e^- annihilations and deep inelastic electron-proton collisions since it is infrared safe at to all orders of perturbative QCD and it can be applied at the parton and hadron level without introducing any additional parameters. In addition, there is no splitting and merging and every particle (or calorimeter tower) is assigned to a jet. However, it must be demonstrate that the K_T algorithm will work in the collider environment where there is an "underlying event". Fig. 2.13 shown that the K_T algorithm works fine at the Tevatron. The parton to hadron correction factors are slightly larger for the K_T algorithm than for the MidPoint algorithm, but the differences are small.
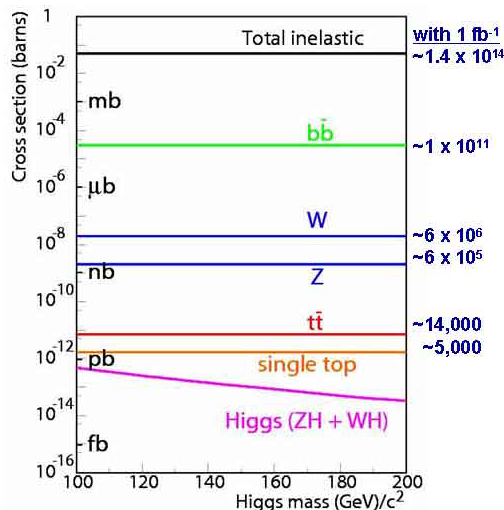

Fig. 3.1. Heavy quark and Boson cross sections for proton-antiproton collisions at 1.96 TeV versus the Higgs mass compared with the total inelastic cross section. Also, shown are the number of events produced with 1 fb^{-1} of integrated luminosity.

III. HEAVY QUARK PHYSICS

At the Tevatron the total inelastic cross section is thousands of times larger than the cross section for producing mesons containing charm or bottom quarks. Nevertheless, as shown in Fig. 3.1, there are lots of events containing charm or bottom mesons. The challenge is to find the heavy quark mesons within the events. At CDF we use a secondary vertex trigger (SVT) to select and save events that contain heavy quark

mesons. Fig. 3.2 shows the published CDF Run 2 prompt charmed meson differential cross sections. The data correspond to about 5.8 pb-1 of integrated luminosity collected with the CDF SVT trigger in two months of running in early 2002. The impact parameter distribution for the charm D^0 mesons is shown in Fig. 3.3. Prompt (i.e. primary) D-mesons extrapolate back to the primary vertex (i.e. the collision point), while secondary D-mesons resulting from decays do not point back to the primary vertex. Most of the reconstructed D-mesons at CDF are prompt (~85%). In Fig. 3.2 and Fig. 3.4 the charmed meson cross sections are compared with FONLL theory predictions [14]. The FONLL approach in perturbative QCD, besides including the next-to-leading order corrections, also provides for the resummation at the next-to-leading log level terms that at large p_T behave like powers of $\log(p_T/m_{charm})$. The FONLL caalculations shown in Fig. 3.2 and Fig. 3.4 also used charm fragmentation functions determined from e^+e^- data. The p_T shapes are consistent with the theory for the D-mesons, but the measured cross sections are about a factor of 1.5 higher than the theory. Although this is within the systematic errors it seems to me that there might be more charm produced at the Tevatron than expected. The next step for CDF will be to measure correlations between charm and anti-charm mesons to learn more about the individual terms contributing to charm production.
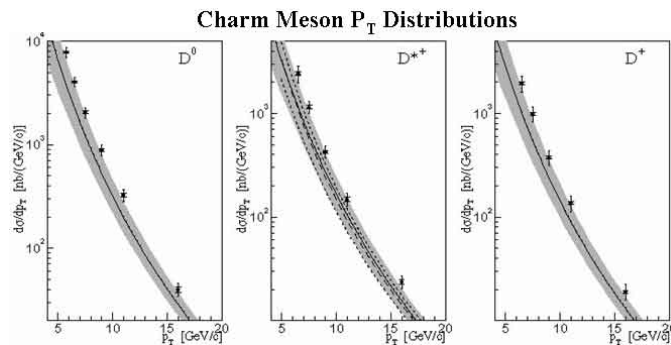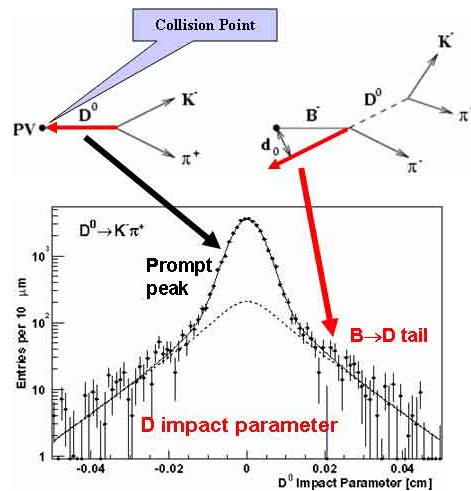

Fig. 3.2. Published CDF Run 2 prompt charmed meson differential cross sections compared with fixed order next-leading-to-leading log (FONLL) theory predictions. The data correspond to about 5.8 pb^{-1} of integrated luminosity collected with the CDF SVT trigger in two months of running in early 2002.

Fig. 3.3. Shows the impact parameter distribution for D^0 mesons in Run 2 at CDF. Prompt (i.e. primary) D-mesons extrapolate back to the primary vertex (i.e. the collision point), while secondary D mesons resulting from decays do not point back to the primary vertex. Most of the reconstructed D-mesons at CDF are prompt (~85%).
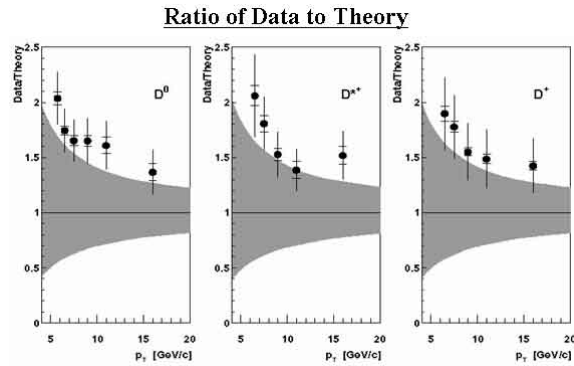
Ratio of Data to Theory

Fig. 3.4. Shows the ratio of data to theory for the charmed meson differential cross sections in Fig. 3.2.

It is important to have good leading order (or leading-log order) estimates of hadron-hadron collider observables. Of course, precise comparisons with data require beyond leading order calculations. If the leading order estimates are within a factor of two of the data, higher order calculations might be expected to improve the agreement. On the other hand, if the leading order estimates are off by more than about a factor of two of the data, one cannot expect higher order calculations to improve the situation. In this case, even if the higher order corrections were large enough to bring agreement, one could not trust a perturbative series in which the second term is greater than the first. If a leading order estimate is off by more than a factor of two, it usually means that one has overlooked some important physics. Fig. 3.5 shows the Tevatron Run 1 data on the integrated b-quark total cross section compared with the QCD Monte-Carlo model predictions for flavor creation (*i.e.* $q + \bar{q} \rightarrow b + \bar{b}$ and $g + g \rightarrow b + \bar{b}$). The leading-log order flavor creation predictions are roughly a factor of four below the data. When I made this plot in 1999 after joining CDF I knew something was "goofy". The leading-log QCD Monte-Carlo cannot be that far off! There must be other leading-log QCD contributions to b-quark production. Also, I did not like the fact that the experimenters extrapolated their data on b-meson production, which is what they measure, back to the parton level (*i.e.* b-quark production). This extrapolation from b-mesons to b-quarks requires an additional assumption about b-quark fragmentation and I believe it is better for the experimenters to present what they measure.
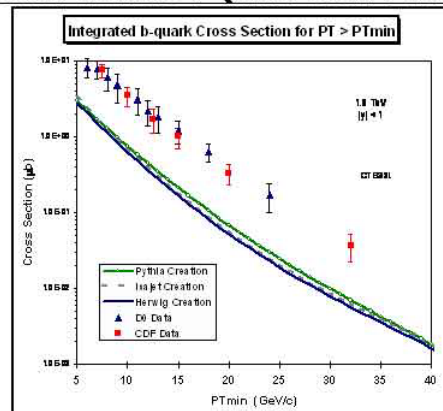
Tevatron Run 1 b-Quark Cross Section

Fig. 3.5. Run 1 Tevatron data on the integrated inclusive b-quark total cross section (p_T > PTmin, |y| < 1) for proton-antiproton collisions at 1.8 TeV compared with the QCD Monte-Carlo model predictions of HERWIG, PYTHIA, and ISAJET for the "flavor creation" subprocess.

Fig. 3.6 shows the Tevatron Run 1 data on the integrated b-quark total cross section compared with the leading-log order QCD Monte-Carlo model predictions from PYTHIA where I included all three sources of b-quarks; flavor creation, flavor excitation, and gluon-splitting [15]. Flavor excitation corresponds to the scattering of a b-quark out of the initial-state into the final-state by a gluon or a light quark via the subprocess $g + b \rightarrow g + b$, $q + b \rightarrow q + b$, or $\bar{q} + b \rightarrow \bar{q} + b$. Flavor excitation is, of course, very sensitive to the number of b-quarks within the proton (*i.e.* the PDF's). The b and $\bar{b}$ quarks are generated through the Q^2 evolution of the structure functions. The number of $b\bar{b}$ pairs within the proton is related, through the Q^2 evolution, to the gluon distribution within the proton. None of the structure functions include "intrinsic" $b\bar{b}$ pairs within the proton (*i.e.* a non-perturbative contribution present a small Q^2). The $b\bar{b}$ pair content within the proton is generated entirely through the Q^2 evolution of the structure functions.

There is another source of b-quarks coming from processes that result in a $b\bar{b}$ pair in the final state but which have no b or $\bar{b}$ -quark in the 2-to-2 hard scattering subprocess. Here the $b\bar{b}$ pair is produced within a parton shower so this source of heavy quarks is referred to as "gluon splitting".
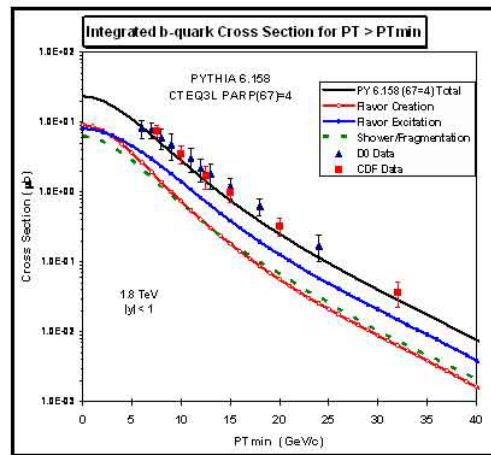

Fig. 3.6. Shows the Tevatron Run 1 b-quark cross sections from Fig. 3.5 compared with the leading-log order QCD Monte-Carlo model predictions of PYTHIA. The four curves correspond to the contribution from flavor creation, flavor excitation, shower/fragmentation (*i.e.* gluon splitting).

At leading-log order within the QCD Monte-Carlo models one can uniquely define three distinct sources of heavy quark production, but at leading order one cannot expect to predict precisely the amount of each source. Nevertheless, it seems clear that at the Tevatron all three sources of b-quark are important. At next-to-leading order the three sources are not uniquely defined. Fig. 3.7 shows the next-to-leading order matrix elements that contribute to the $gg \rightarrow Q\bar{Q}g$ cross section. At the amplitude level one can identify flavor creation, flavor excitation, and gluon splitting, but the cross section is the absolute value squared of the sum of three amplitudes and there are interference terms. It is still useful to think in terms of these three sources. Each of the three sources has a distinct topology and can be studied more closely by studying correlations between the outgoing b and $\bar{b}$ mesons.
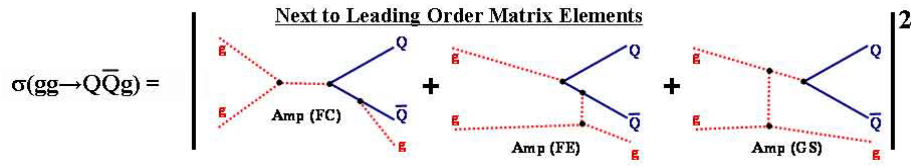
Fig. 3.7. Shows the heavy flavor next-to-leading order amplitudes for $gg \rightarrow Q\bar{Q}g$ corresponding to flavor creation (FC), flavor excitation (FE), and gluon splitting (GS). The cross section is the absolute value squared of the sum of the amplitudes.

Fig. 3.8 shows the CDF Run 2 differential cross sections for producing b-mesons compared with a perturbative QCD FONLL calculation [16]. Here the data and theory are compared at the b-meson level and the theory agrees quite well with the data.
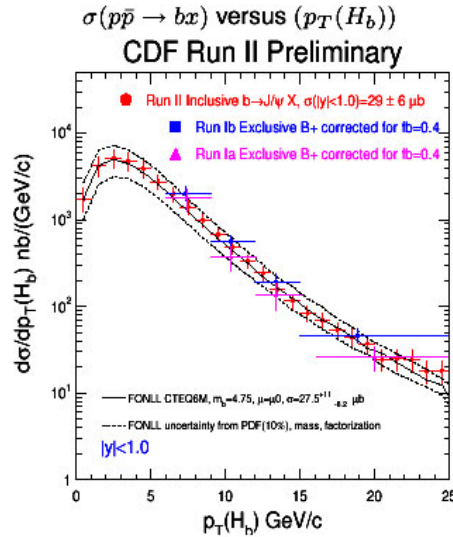

Fig. 3.8. CDF Run 2 differential cross sections for producing b-hadrons, H_b, with $|y| < 1$ in proton-antiproton collisions at 1.96 TeV with an integrated luminosity of 39.7 pb^{-1}. The cross section is plotted versus the transverse momentum of the b-hadron and compared with a next-to-leading order QCD calculation.
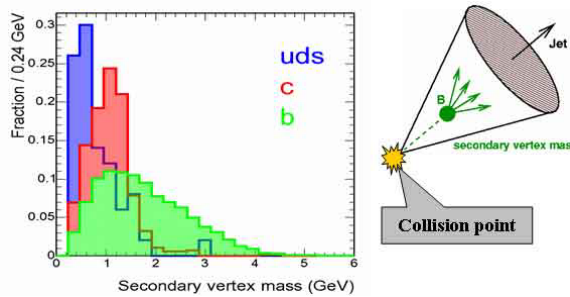
Fig. 3.9. (*right*) CDF b-jets are identified by studying the invariant mass of the charged particles emanating from the secondary vertex which is displaced slightly from the primary interaction vertex due to the long lifetime of the heavy b-quark. (*left*) Shows the invariant mass distributions for b-quark jets, c-quark jets, and light quark jets predicted by PYTHIA Tune A.

In addition to studying b-meson production one can study the production of b-quark jets (*i.e.* jets containing a b-meson). As illustrated in Fig. 3.9, b-jets are identify by studying the invariant mass of the charged particles emanating from the secondary vertex which is displaced slightly from the primary interaction vertex due to the long lifetime of the heavy b-quark. Fig. 3.10 shows the resulting CDF b-jet inclusive cross section at 1.96 TeV and in Fig. 3.11 the data are compared with a next-to-leading order QCD calculation and with PYTHIA Tune A. PYTHIA Tune A has been tuned

to fit the CDF Run 1 "underlying event" data by adjusting the multiple-parton interactions. I will discuss the QCD Monte-Carlo generator tunes in Section V. The data are about a factor of 1.4 higher than both the leading-log estimate from PYTHIA Tune A and the NLO calculation. However, the NLO calculation has a large uncertainty due to the choice of scale.
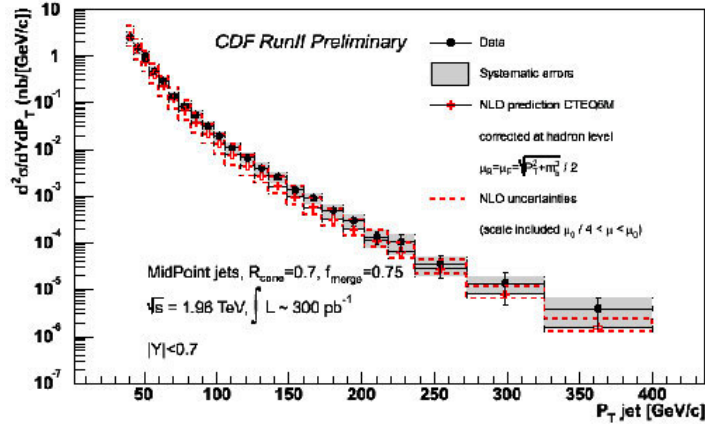

Fig. 3.10. Shows the CDF Run 2 b-jet inclusive cross section in proton-antiproton collisions at 1.96 TeV with an integrated luminosity of 300 pb^{-1}. The data are plotted versus the P_T of the b-jets and are compared with a NLO QCD calculation.
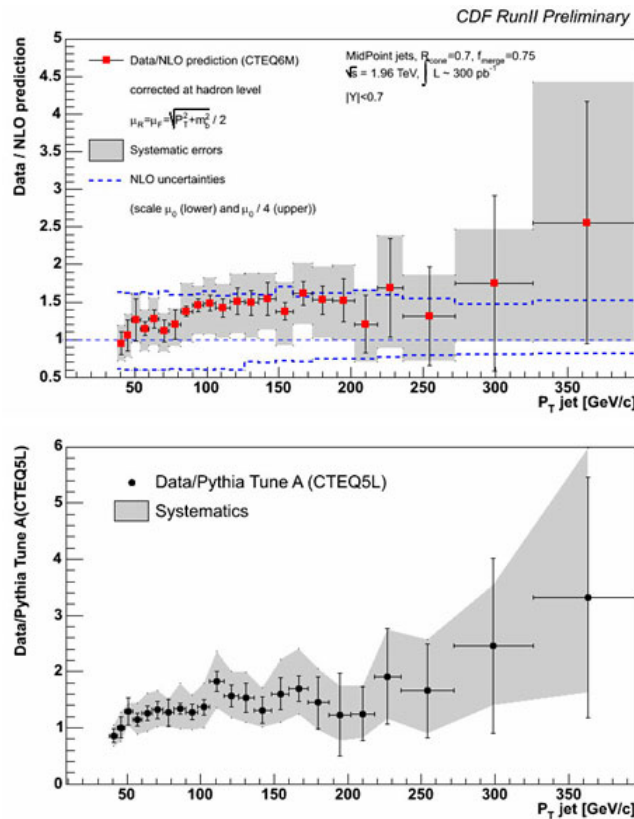
Fig. 3.11. Shows a comparison of the CDF Run 2 b-jet inclusive cross section from Fig. 2.12 with a NLO QCD prediction (top) and with PYTHIA Tune A (bottom). The plots show the ratio of data to theory.

   The b-jet data in Fig. 3.10 have been corrected to the hadron (*i.e.* particle level) and the "jets" include contributions from the "underlying event". The NLO theory has been corrected to the hadron level by adding in the effects of the "underlying event" and hadronization. It is surprising that the NLO theory (when corrected to the hadron

level) is so similar to the predictions of PYTHIA Tune A. The data/theory for both is about 1.4.

Fig. 3.12 shows the CDF Run 2 $b\bar{b}$ dijet invariant mass distribution at 1.96 TeV compared with PYTHIA Tune A, HERWIG, and MC@NLO [17] and Table 3.1 shows the integrated $b\bar{b}$ dijet cross section. PYTHIA Tune A fits the data better than HERWIG or MC@NLO. This is because PYTIA Tune A has been tuned to fit the "underlying event" at the Tevatron by adjusting the multiple-parton interactions. HERWIG and MC@NLO (which uses HERWIG) do not include multiple-parton interactions and do not have enough activity in the "underlying event". JIMMY [18] is a model of multiple parton interaction which can be combined with HERWIG (and MC@NLO) to enhance the "underlying event" thereby improving the agreement with data. When JIMMY is added to MC@NLO then agreement is improved. Both the inclusive jet cross section and the b-jet cross section are sensitive to the "underlying event".

Fig. 3.12 also shows the b -jet $\bar{b}$ -jet $\Delta\phi$ distribution compared with PYTHIA Tune A, HERWIG, and MC@NLO. PYTHIA Tune A and MC@NLO do a good job in describing the $b\bar{b}$ $\Delta\phi$ distribution. It is not an accident that PYTHIA Tune A roughly agrees with the data. I tuned the initial-state radiation in PYTHIA Tune A (*i.e.* PARP(67)) to agree with the CDF Run 1 $b\bar{b}$ $\Delta\phi$ distribution [19]. PARP(67) sets the high p_T scale for initial-state radiation and increasing it increases the amount of high p_T initial state-radiation in PYTHIA (see Section V). For MC@NLO the agreement is a prediction. For PYTHIA Tune A the agreement is a "tune", but it does show consistency between the CDF Run 1 analysis and the preliminary Run 2 results.
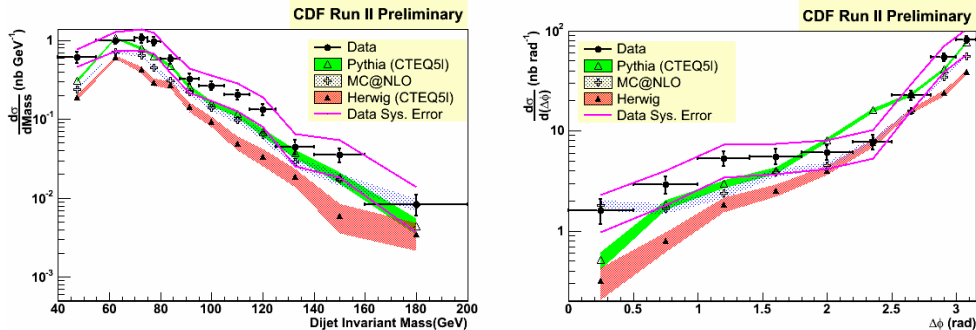

Fig. 3.12. Shows the CDF Run 2 $b\bar{b}$ dijet invariant mass distribution (left) and the b -jet $\bar{b}$ -jet $\Delta\phi$ distribution (right) at 1.96 TeV compared with PYTHIA Tune A, HERWIG, and MC@NLO.

Table 3.1. The CDF Run 2 integrated $b\bar{b}$ dijet cross section (E_T(b-jet#1) > 30 GeV, E_T(b-jet#2) > 20 GeV, $|\eta$(b-jets)$|$ < 1.2) at 1.96 TeV compared with PYTHIA Tune A, HERWIG, MC@NLO, and MC@NLO + JIMMY.

CDF (preliminary)	$34.5 \pm 1.8 \pm 10.5$ nb
PYTHIATuneA (CTEQ5L)	38.7 ± 0.6 nb
HERWIG (CTEQ5L)	21.5 ± 0.7 nb
MC@NLO	28.5 ± 0.6 nb
MC@NLO+ JIMMY	35.7 ± 2.0 nb

The top quark was discovered at the Tevatron by CDF and DØ in 1995 and in the last 10 years both experiments have continued to improve on the precision of their measurements. The top quark cross section is now measured to an accuracy of about 12% and the top mass is measured to about 2%. At the Tevatron about 15% of the $t\bar{t}$ pairs are produced by gluon fusion and about 85% from quark-antiquark annihilation.

Both CDF and DØ now have hundreds of top quark events and are beginning to study the detailed properties of the top quark (*i.e.* charge, lifetime, branching fractions, etc.).

The top quark is heavier than a W-boson plus a b-quark so it decays very quickly via the mode t→W+b. In fact the decay is so rapid that it decays into W+b before it hadronizes. The b-quark fragments into a b-jet and the W-boson decays either leptonically into a lepton and a neutrino (~11% per flavor) or hadronically into a quark-antiquark pair (~67% all flavors) resulting in the $t\bar{t}$ decay channels shown in Fig. 3.13. The dilepton channel corresponds to both the top and anti-top decaying into a lepton, neutrino, and a b-jet. The lepton+jets channel corresponds to one top quark decaying into a lepton, neutrino, and a b-jet and the other top quark decaying into a b-jet plus two light quark jets. The all jets channel occurs when both top quarks decay into a b-jet plus two light quark jets.
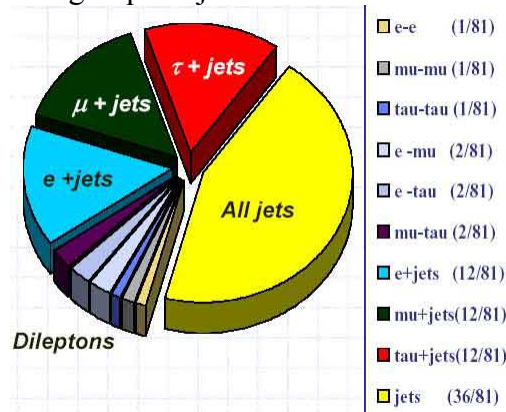
Fig. 3.13. Pie chart showing decay channels of $t\bar{t}$ quark pairs produced in hadron-hadron collisions.

The smallest cross section times branching fraction is the dilepton channel. Fig. 3.14 shows the number of CDF Run 2 $t\bar{t}$ dilepton candidate events in a data sample with an integrated luminosity of 750 pb^{-1}. The events are required not to contain a Z-boson and to have two leptons with $p_T > 20$ GeV/c and missing transverse energy, ME$_T$, greater than 25 GeV. Requiring opposite sign leptons, and ≥2 jets with E$_T > 15$ GeV, and H$_T > 200$ GeV, yields 65 events with an estimated background of about 20 events and gives a $t\bar{t}$ total cross section of about 8.3 pb. Note that

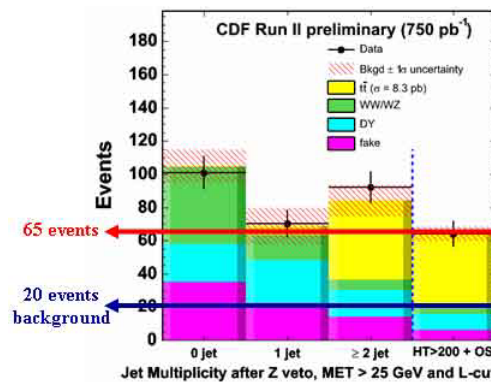$$H_T = \sum_{leptons} p_T + \sum_{jets} E_T + ME_T.$$

Fig. 3.14. Shows the number of CDF Run 2 $t\bar{t}$ dilepton candidate events in proton-antiproton collisions at 1.96 TeV in a data sample with an integrated luminosity of 750 pb^{-1}. The events are required not to contain a Z-boson and to include two leptons with $p_T > 20$ GeV/c and missing transverse energy greater than 25 GeV. The plot shows the number of events with 0, 1, and ≥2 jets (first three bins). Further requiring ≥2 jets, H$_T > 200$ GeV, and

opposite sign leptons (last bin) yields 65 events with an estimated background of about 20 events and gives a measured $t\bar{t}$ total cross section of about 8.3 pb.

Fig. 3.15 shows the number of CDF Run 2 $t\bar{t}$ lepton+jets candidate events in a data sample with an integrated luminosity of 695 pb^{-1}. The events are required to contain a W-boson and to have H_T > 200 GeV and to have at least one b-tagged jet. Requiring W + ≥4 jets yields about 150 events with a small background resulting in a $t\bar{t}$ total cross section of about 8.2 pb As shown in Fig. 3.16, requiring two b-tagged jets and W + ≥4 jets yields about 45 events with almost no background and gives a $t\bar{t}$ total cross section of about 8.8 pb.
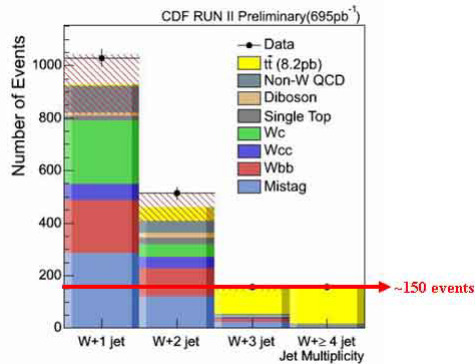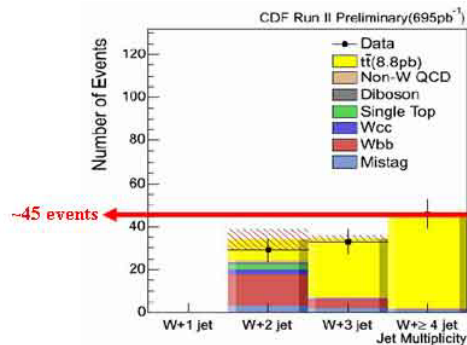

Fig. 3.15. Shows the number of CDF Run 2 top-quark lepton+jets candidate events in proton-antiproton collisions at 1.96 TeV with an integrated luminosity of 695 pb^{-1}. The events are required to contain a W-boson and to have H_T > 200 GeV and to have at least one b-tagged jet. The plot shows the number of events with a W-boson plus 1, 2, 3, and ≥4 jets. Requiring W + ≥4 (last bin) yields about 150 events with a small background resulting in a $t\bar{t}$ total cross section of about 8.2 pb.

Fig. 3.16. Shows the number of CDF Run 2 top-quark lepton+jets candidate events in proton-antiproton collisions at 1.96 TeV with an integrated luminosity of 695 pb^{-1}. The events are required to contain a W-boson and to have H_T > 200 GeV and to have two b-tagged jets. The plot shows the number of events with a W-boson plus 2, 3, and ≥4 jets. Requiring W + ≥4 jets (last bin) yields about 45 events with almost no background resulting in a $t\bar{t}$ total cross section of about 8.8 pb.
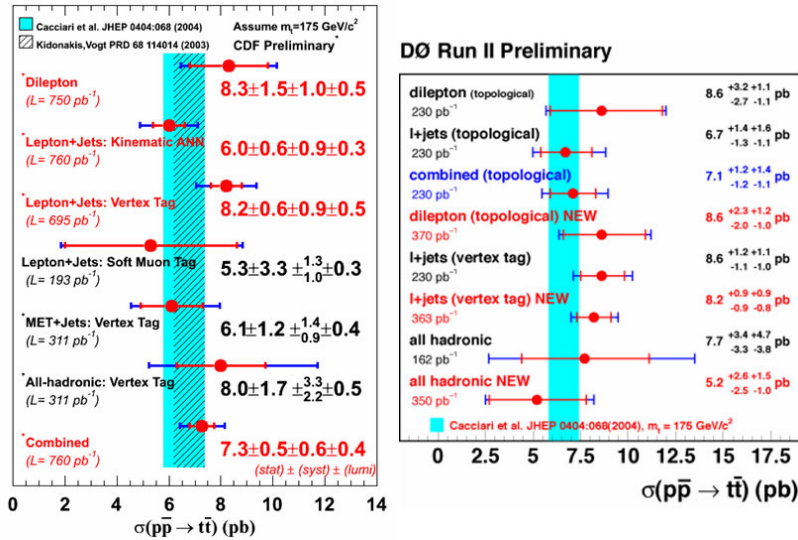
Fig. 3.17. Summary of various Run 2 Tevatron measurements of the $t\bar{t}$ total cross section assuming a top quark mass of 175 GeV/c^2. The theoretical prediction of $6.7^{+0.7}_{-0.9}$ pb is also shown [20].

Fig. 3.17 summarizes the various Tevatron Run 2 measurements of the $t\bar{t}$ total cross section and Fig. 3.18 summarizes the CDF top mass measurements. Fig. 3.19 shows the errors on the CDF combined $t\bar{t}$ total cross section and top quark mass measurements from last summer with 350 pb^{-1} of data together with the improved result with 760 pb^{-1} presented at the winter conferences earlier this year. As shown in Fig. 3.20 the largest source of systematic error on the t-quark mass is the uncertainty in the jet energy scale. As the integrated luminosity increases we expect the uncertainty in the jet energy scale will decrease allowing for a more precise top mass measurement. Currently the uncertainty on the top quark mass is around 2.8 GeV. we hope to eventually achieve an uncertainty of about 1.5 GeV (*i.e.* a 1% measurement!).
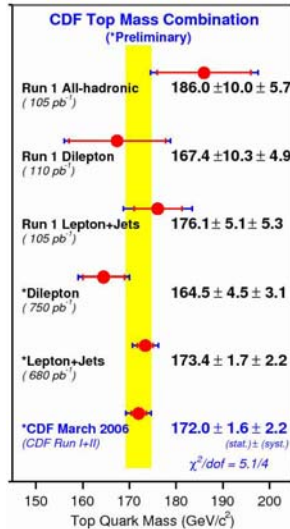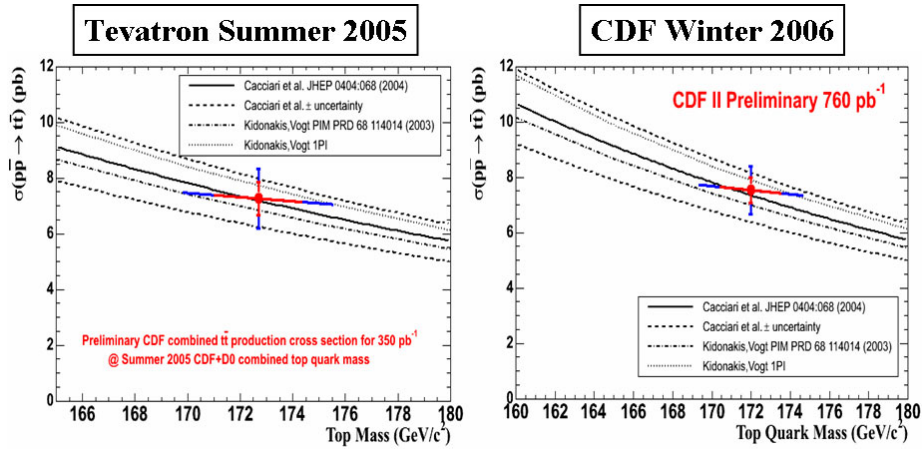

Fig. 3.18. Summary of various CDF measurements of the top quark mass measurements as of March 2006.

Fig. 3.19. Shows the errors on the CDF combined $t\bar{t}$ total cross section and top quark mass measurements from last summer with 350 pb[-1] of data (*left*) together with the improved result with 760 pb[-1] presented at the winter conferences earlier this year (*right*).

Fig. 3.21 and Fig. 3.22 show the CDF search for $t\bar{t}$ resonances. Fig. 3.21 shows the $t\bar{t}$ invariant mass distribution from Run 1 and from Run 2 with an integrated luminosity of 319 pb[-1], and Fig. 3.22 shows the most recent CDF $t\bar{t}$ invariant mass distribution from Run 2 with an integrated luminosity of 682 pb[-1]. The Run 1 data and the early Run 2 data show an intriguing structure in the top-pair invariant mass distribution around 500 GeV (*i.e.* an excess of events which might be evidence for a $t\bar{t}$ resonance!). This structure seems to be disappearing with the increased statistics in Fig. 3.22. However, the most recent distribution still looks a little peculiar. Fig. 3.22 contains 447 $t\bar{t}$ pairs and it will be very interesting to see how the plot looks with twice as many pairs.
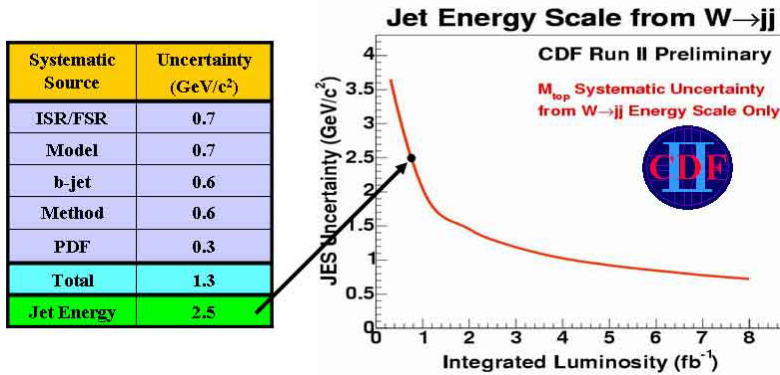

Fig. 3.20. Shows the sources of systematic errors on the t-quark mass measurement from CDF. The largest uncertainty in the jet energy scale.
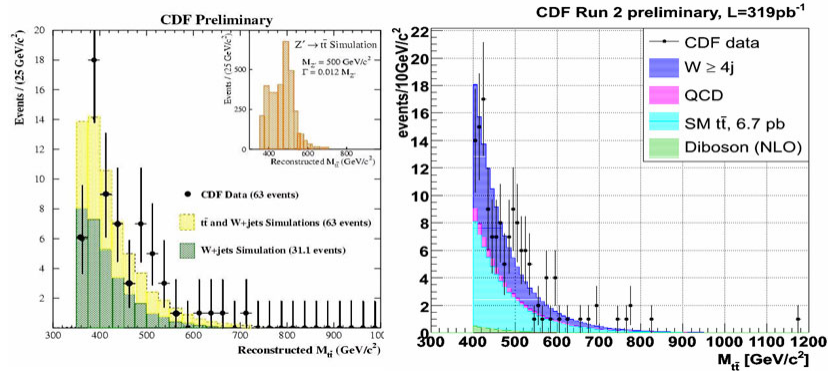
Fig. 3.21. Shows the CDF $t\bar{t}$ invariant mass distribution from Run 1 (*left*) and from Run 2 with an integrated luminosity of 319 pb^{-1} (*right*).
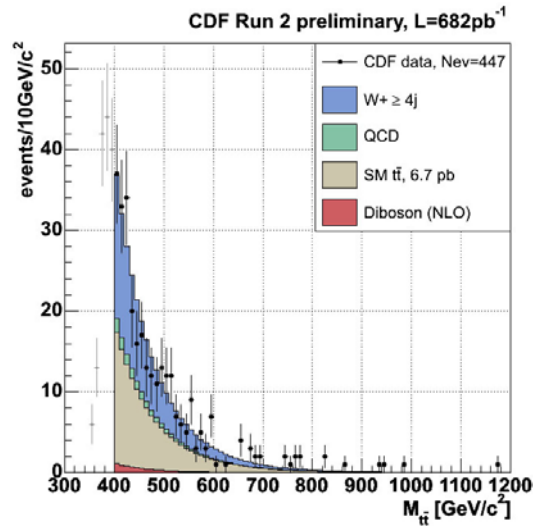

Fig. 3.22. Shows the most recent CDF $t\bar{t}$ invariant mass distribution from Run 2 with an integrated luminosity of 682 pb^{-1}.
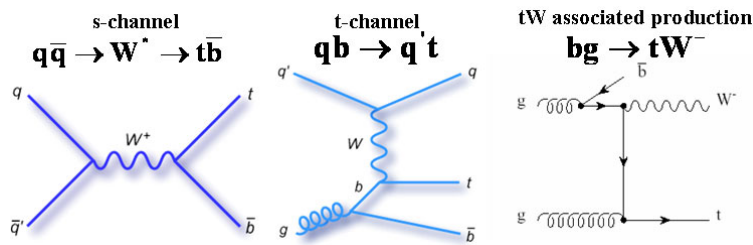

Fig. 3.23. Sources of single top production at the Tevatron. Single top quarks can be produced through s or t-channel W-boson exchange or produced in association with a top quark and a W-boson.

Top anti-top pairs are produced strongly at the Tevatron with a total cross section of around 7 pb. Single top quarks are produced weakly with an expected cross section of around 2 pb [21]. Fig. 3.23 shows the sources of single top quark production at the Tevatron. Single top quarks can be produced through s or t-channel W-boson exchange or produced in association with a top quark and a W-boson. Both CDF and DØ are vigorously working to observe single top production. At present the upper limits are around 3 pb as shown in Fig. 3.24. We are very close to seeing single top

production at the Tevatron. Certainly it should be seen with 2 fb^{-1} which might be obtained next year.

95% C.L. limits on single top cross-section		
Channel	CDF (696 pb^{-1})	DØ (370 pb^{-1})
Combined	3.4 pb (2.9 pb)	
s-channel	3.2 pb (0.9 pb)	5.0 pb
t-channel	3.1 pb (2 pb)	4.4 pb

Fig. 3.24. Tevatron limits at 95% confidence level on single top production at 1.96 TeV for s-channel production, t-channel production, and combined. The theory predictions are shown in parentheses [21].

All the heavy quark cross sections at the Tevatron, charm meson, b-meson, b-jet, and top seem to me to be a bit larger than expected from theory. Charm meson by a factor of about 1.5 and the inclusive b-jet cross section by about 1.4. Top quark production is within 10% of the theory, but again on the high side. True, all of these discrepancies are within the systematic uncertainties of the data. However, I feel there may still be more to be learned about heavy quark production in hadron-hadron collisions. I hope the Higgs cross section is also larger than expected!
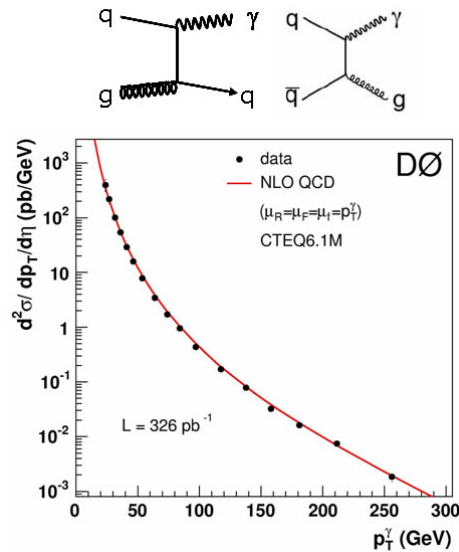

Fig. 4.1. DØ Run 2 direct photon differential cross sections for proton-antiproton collisions at 1.96 TeV with an integrated luminosity of 326 pb^{-1}. There highest p_T photon is 442 GeV/c with three events above 300 GeV/c. The data are compared with a NLO QCD theory calculation using CTEQ6.1M.
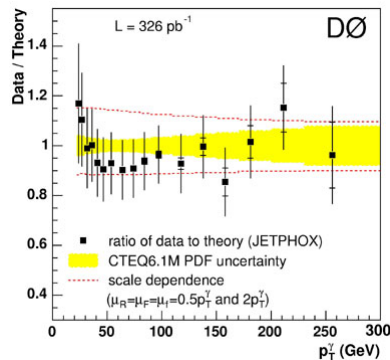

Fig. 4.2. Data divided by theory for the DØ Run 2 direct photon cross sections shown in Fig. 4.1.

IV. PHOTONS AND BOSONS

Fig. 4.1 shows the DØ Run 2 direct photon differential cross sections together with the leading order Feynman diagrams. There highest p_T photon is 442 GeV/c with three events above 300 GeV/c! In Fig. 4.2 the data are compared with a next-to-leading order QCD calculation. The agreement between theory and experiment is very good except maybe at small p_T where the data rise above the theory. It has always been difficult to explain the excess in photons at small p_T at the Tevatron. In a Run 1 analysis, CDF was able to fit the data, but it required assigning the incoming partons a very large intrinsic transverse momentum [22].

Fig. 4.3 shows the CDF Run 2 cross sections for γ+c and γ+b production in proton-antiproton collisions compared with PYTHIA Tune A. PYTHIA predicts the relative amounts of γ+c and γ+b correctly. Fig. 4.4 shows the CDF di-photon invariant mass spectrum at 1.96 TeV. It agrees well with the expectations from perturbtive QCD.
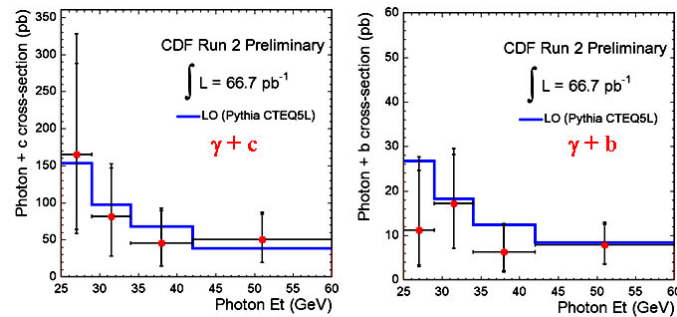

Fig. 4.3. CDF Run 2 cross sections for γ+c and γ+b production in proton-antiproton collisions at 1.96 TeV with an integrated luminosity of 66.7 pb[-1]. The data are compared with PYTHIA Tune A using CTEQ5L. The integrated total cross sections for $E_T(\gamma)$ > 25 GeV are σ(γ+c) = 486.2±152.9(stat)+86.5(sys)-90.9(sys) pb and σ(γ+b) = 40.6±19.5(stat)+7.4(sys)-7.8(sys) pb.
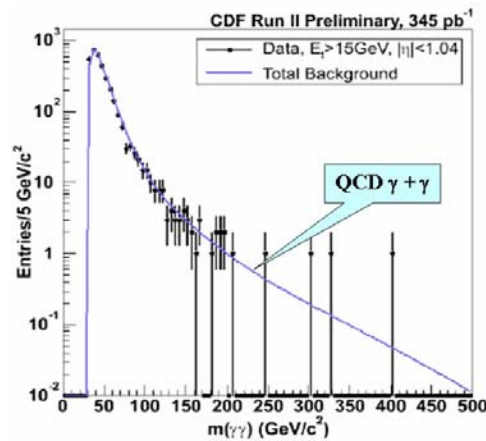

Fig. 4.4. CDF Run 2 measurement of two-photon production in proton-antiproton collisions at 1.96 TeV with an integrated luminosity of 345 pb[-1] versus the two-photon invariant mass. The shape of the data are compared with the two-photon spectrum expected from perturbative QCD (labeled as "background").
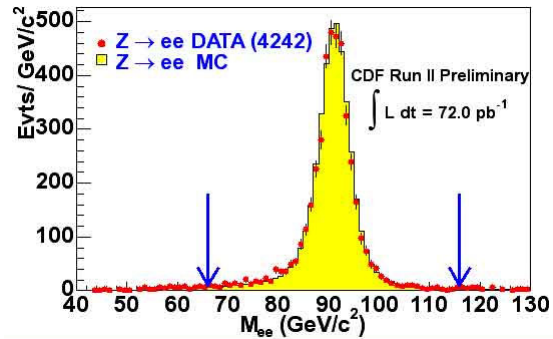
Fig. 4.5. CDF Run 2 measurement of Z-boson production in proton-antiproton collisions at 1.96 TeV with an integrated luminosity of 72 pb^{-1}. The plot shows the shape of the invariant mass spectrum of e^+e^- pairs with 4242 events in the range $67 < M_{ee} < 117$ GeV compared with PYTHIA Tune AW. The Z-boson cross section at the Tevatron agrees well with NNLO theory.
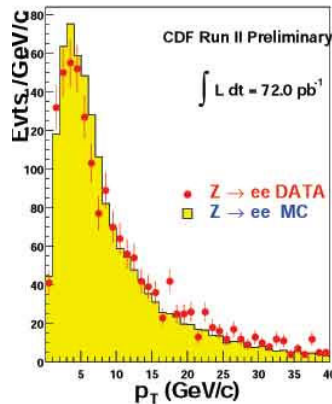

Fig. 4.6. CDF Run 2 measurement of Z-boson transverse momentum distribution in proton-antiproton collisions at 1.96 TeV with an integrated luminosity of 72 pb^{-1}. The plot shows the shape of the p_T distribution of e^+e^- pairs with $67 < M_{ee} < 117$ GeV from Fig. 3.5 compared with PYTHIA Tune AW.

Fig. 4.5 shows the invariant mass spectrum of e^+e^- pairs near the Z-boson mass and Table 4.1 gives the Z-boson total cross section measured by CDF. With 72 pb^{-1} of data CDF has 4242 Z-boson events in the range $67 < M_{ee} < 117$ GeV. Fig. 4.6 shows the Z-boson transverse momentum distribution compared with PYTHIA Tune AW and Fig. 4.7 shows the Drell-Yan electron-pair invariant mass spectrum out to 450 GeV/c^2 measured by CDF. Tune AW is a Run 2 PYTHIA 6.2 tune that fits the p_T distribution of the Z-boson as well as the CDF "underlying event" data (see Section V). Fig. 4.8 shows a summary of the CDF Run 2 measurements of the Z-boson cross section (times branching fraction) in proton-antiproton collisions at 1.96 TeV for $Z \rightarrow e^+e^-$, $Z \rightarrow \mu^+\mu^-$, and $Z \rightarrow \tau^+\tau^-$ compared with the next-to-next-to-leading order (NNLO) theory prediction [23]. The Z-boson cross section at the Tevatron agrees well with NNLO theory.
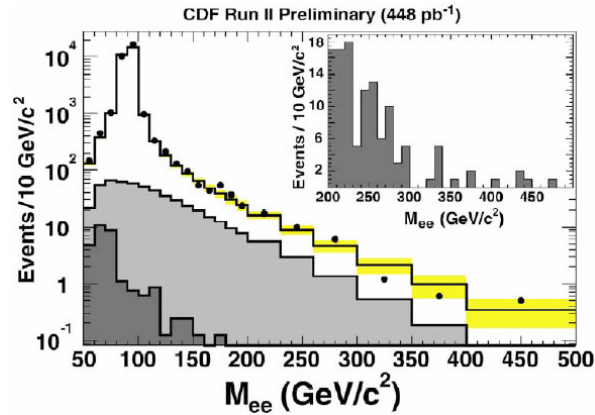
Fig. 4.7. CDF Run 2 measurement of Drell-Yan lepton-pair production in proton-antiproton collisions at 1.96 TeV with an integrated luminosity of 448 pb^{-1}. The plot shows the shape of the invariant mass spectrum of e$^+$e$^-$ pairs compared with PYTHIA Tune AW.

Both CDF and DØ have worked hard to develop techniques for detecting tau leptons so that they can reconstruct the $\tau^+\tau^-$ invariant mass spectrum. As illustrated in Fig. 4.9 this allows one not only to see Z→$\tau^+\tau^-$, but also to search for Higgs→$\tau^+\tau^-$ production. Fig. 4.10 shows the CDF Run 2 measurement of Z→$\tau^+\tau^-$ production, where one of the τ's decays hadronically and one decays leptonically. The leptonic tau decay is identified by observing the lepton and missing transverse energy. The hadronic tau decay produces a "mini-jet" sometimes consisting of a π^0 plus several charged pions. As illustrated in Fig. 4.11, this cluster of pions is required to be in a 10° cone which is isolated within a 30° cone. CDF uses its Central Electron Shower detector (CES) to identify π^0's, photons, and electrons. The CES measures the shape of the shower produced when one of these particles hits the detector. Fig. 4.12 shows a search for Higgs→$\tau^+\tau^-$ at CDF using these techniques.

Table 4.1. CDF Run 2 results on the cross section times branching fraction for W and Z bosons in proton-antiproton collisions at 1.96 TeV. The W-boson cross section is measured using electrons from the central and forward region of the detector. The data are compared with NNLO theory calculations [23].

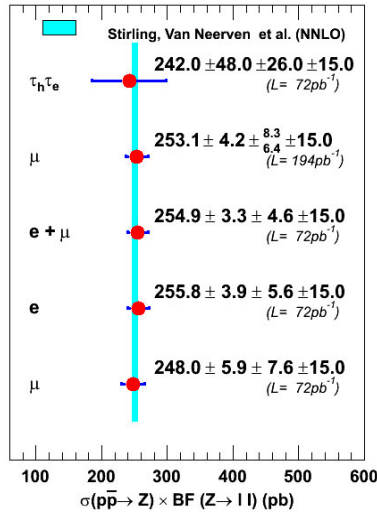|	CDF Data (1.96 TeV)	NNLO Theory
$\sigma(Z{\to}e^+e^-)$	254.9±3.3(stat) ±4.6(sys) ±15.2(lum) pb	252.3±5.0 pb
$\sigma(Z{\to}\tau^+\tau^-)$	265±20(stat) ±21(sys) ±15(lum) pb	252.3±5.0 pb
$\sigma(W{\to}e\nu)^{forward}$	2815±13(stat) ±94(sys) ±169(lum) pb	2687±54 pb
$\sigma(W{\to}e\nu)^{central}$	2775±10(stat) ±53(sys) ±167(lum) pb	2687±54 pb
$\sigma(W{\to}e\nu)/\sigma(Z{\to}e^+e^-)$	10.92±0.15(stat) ±0.14(sys)	10.69±0.08

Fig. 4.8. Summary of the CDF Run 2 measurements of the Z-boson cross section (times branching fraction) in proton-antiproton collisions at 1.96 TeV for $Z \rightarrow e^+e^-$, $Z \rightarrow \mu^+\mu^-$, and $Z \rightarrow \tau^+\tau^-$ compared with the NNLO theory prediction [22].
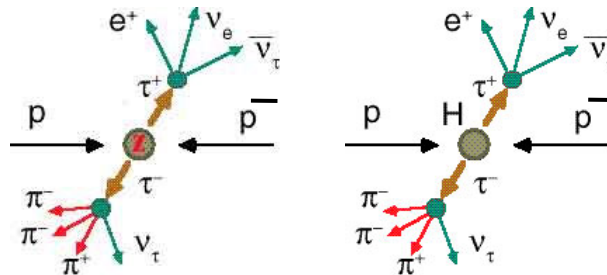

Fig. 4.9. Shows the production of a Z-boson (*left*) or a Higgs-boson (*right*) in proton-antiproton collisions in which the Z-boson (or Higgs-boson) subsequently decays into a $\tau^+\tau^-$ pair where one of the τ's decays hadronically and one decays leptonically.
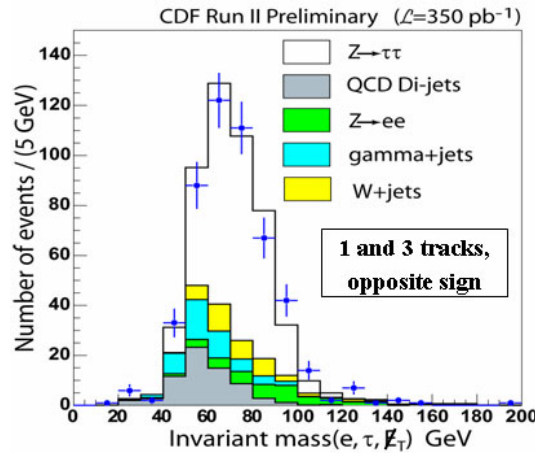

Fig. 4.10. CDF Run 2 measurement of $Z \rightarrow \tau^+\tau^-$ production in proton-antiproton collisions at 1.96 TeV with 316 candidate events with an integrated luminosity of 350 pb^{-1}. The plot shows the shape of the invariant mass spectrum of a τ-lepton reconstructed from its decay into a π^0 plus one or three charged tracks combined with an electron from leptonic decay of a second τ-lepton and the missing energy.
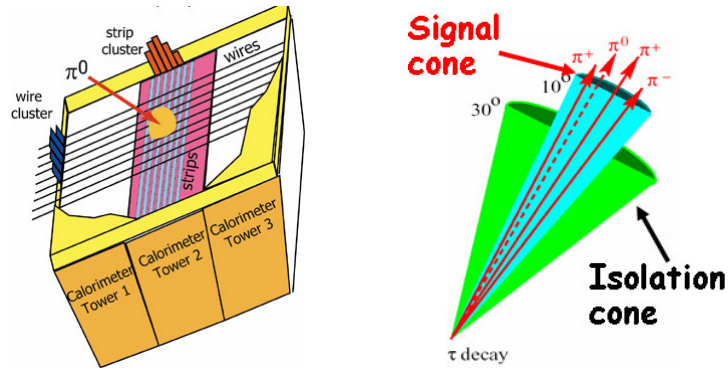
Fig. 4.11.(*left*) Illustration of the CDF Central Electron Shower detector (CES). The CES is used to identify π^0's, photons, and electrons. (*right*) Show the "signal" cone (10°) and the "isolation" cone (30°) used to identify τ-leptons that decay into a "mini-jet" consisting of a π^0 plus several charged pions.
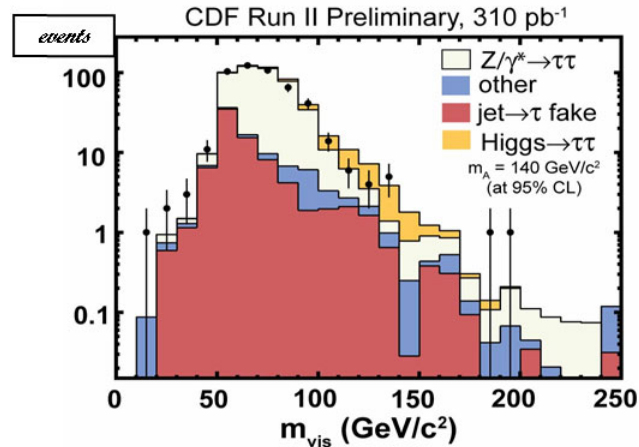

Fig. 4.12. CDF Run 2 measurement of the shape of the reconstructed $\tau^+\tau^-$ invariant mass spectrum in proton-antiproton collisions at 1.96 TeV with an integrated luminosity of 310 pb^{-1}. The data exclude a 140 GeV/c^2 Higgs$\to\tau^+\tau^-$ within the MSSM scenario at a 95% confidence level.
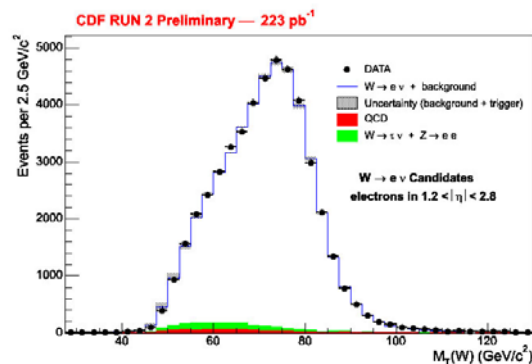

Fig. 4.13. CDF Run 2 measurement of W-boson production in proton-antiproton collisions at 1.96 TeV with an integrated luminosity of 223 pb^{-1}. There are 48,144 W candidates with a background of about 4.5%. The plot shows the shape of the transverse mass spectrum constructed from and electron in the forward region of the CDF detector $1.2 < |\eta| < 2.8$ and the missing transverse energy.

Fig. 4.13 shows a recent CDF measurement of the W-boson cross section at the Tevatron which uses electrons in the forward region of the CDF detector $1.2 < |\eta| < 2.8$. Table 4.1 compares the forward electron result with a previous measurement which used electrons in the central region. At the 1.96 TeV, the W$\to$eν cross section is about 11 times larger than the Z$\to$e$^+$e$^-$ cross section. The branching fraction for

$Z \rightarrow e^+e^-$ is about 3.4%, whereas the $W \rightarrow e\nu$ branching fraction is about 3.2 times larger (about 11%). Hence, the overall W/Z production ratio is around 3.4 at 1.96 TeV. A summary of 20 years of measuring W-boson and Z-boson production at hadron-hadron colliders is shown in Fig. 4.14.
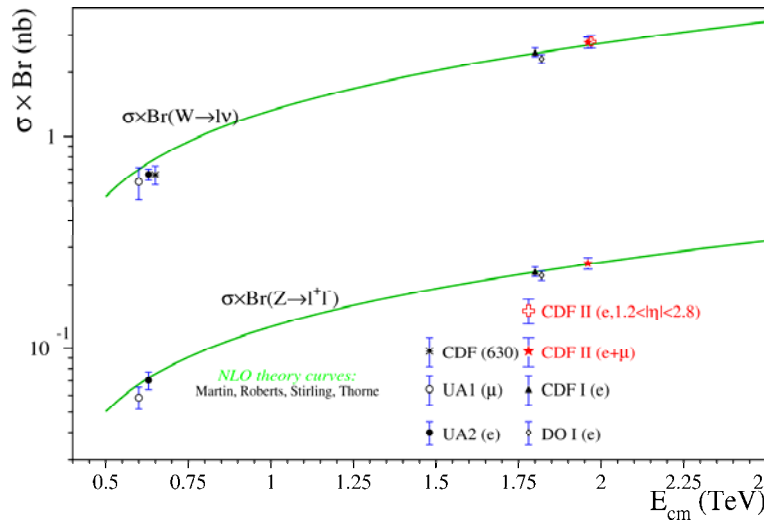

Fig. 4.14. Summary of 20 years of measuring W-boson and Z-boson production at hadron-hadron colliders.

Fig. 4.15. Leading order Feynman diagrams for producing a Z-boson in association with a heavy quark, Q, at hadron-hadron colliders.
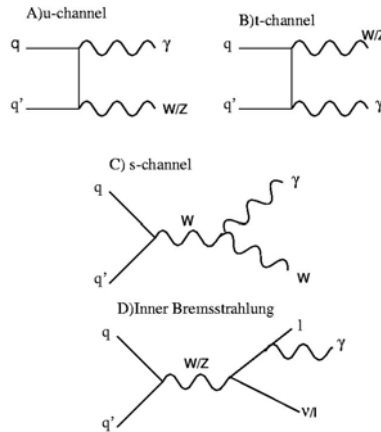

Fig. 4.16. Leading order Feynman diagrams for producing W+γ and Z+γ in proton-antiproton collisions.

An interesting process to study at the Tevatron is the production of a Z-boson in association with a heavy quark. The leading order Feynman diagrams are shown in Fig. 4.15. The Z+b-jet cross section is very sensitive to the number of b-quarks within the proton, similar to b-quark flavor excitation which I discussed in Section III. The Z+b-jet cross section is, therefore, a good measurement of the amount of b-quarks within the proton. This process is also an important background for new physics. In

a recent analysis CDF measured the Z+b-jet cross section at 1.96 TeV to be $\sigma(Z+b\text{-jet})$ = 0.96±0.32(stat)±0.14(sys) pb for P_T(jet) > 20 GeV. Here CDF extracted the fraction of tagged b-jets from the secondary vertex mass distribution using the techniques I discussed in the previous Section (see Fig. 3.9). The NLO theory prediction is about 0.52 pb. CDF also measured the ratio of Z+b-jet to Z+jet to be 0.0237±0.0078(stat)±0.0033(sys) with NLO theory predicting about 0.018.

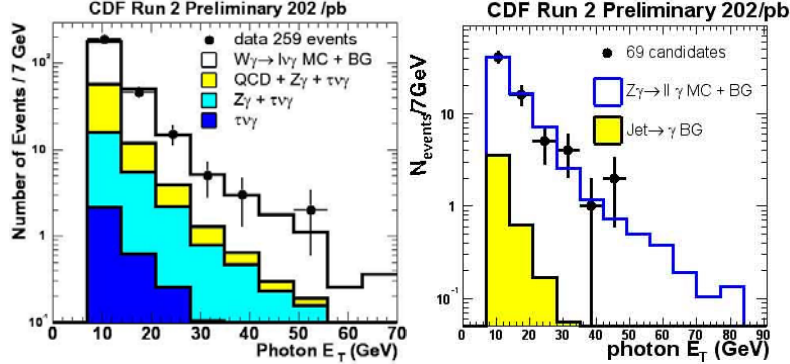**Fig. 4.17**. CDF Run 2 measurement of W+γ (259 events, *left*) and Z+γ (69 events, *right*) production in proton-antiproton collisions at 1.96 TeV with an integrated luminosity of 202 pb^{-1}. The plot shows the shape of the photon transverse energy spectrum compared with QCD theory predictions.

Both CDF and DØ are measuring the rate of producing two vector bosons at the Tevatron (*i.e.* di-boson production). The leading order Feynman diagrams for producing W+γ and Z+γ in proton-antiproton collisions are shown in Fig. 4.16 and the CDF Run 2 data are shown in Fig. 4.17. Table 4.2 compares the measured cross-sections with the NLO theory predictions [24]. Note that at 1.96 TeV $\sigma(W)/\sigma(Z) \approx$ 3.4 while $\sigma(W+\gamma)/\sigma(Z+\gamma) \approx 1.2$! This is an interesting quantum mechanical effect due to the fact that the s-channel amplitude in Fig. 4.16 is absent for Z+γ production. For W+γ production the s-channel amplitude interferes destructively with the t and u-channel amplitudes which suppresses W+γ production relative to Z+γ production.

Table 4.2. CDF Run 2 results on the cross section two vector bosons in proton-antiproton collisions at 1.96 TeV. The W-boson cross section is measured using electrons from the central and forward region of the detector. The data are compared with NLO theory calculations [24].

	CDF Data (1.96 TeV)	NLO Theory
$\sigma(W+\gamma)\times B_F(W\rightarrow l\nu)$	19.7±1.7(stat) ±2.0(sys) ±1.1(lum) pb	19.3±1.4 pb
$\sigma(Z+\gamma)\times B_F(Z\rightarrow l\,l)$	5.3±0.6(stat) ±0.3(sys) ±0.3(lum) pb	5.4±0.3 pb
$\sigma(W+W)$ (825 pb^{-1})	13.7±2.3(stat) ±1.6(sys) ±1.2(lum) pb	12.4±0.8 pb
$\sigma(W+Z)$ (825 pb^{-1})	< 6.34 pb (95% CL)	3.7±0.1 pb

Mode	ee	eμ	μμ	ll
WW	12.82 ± 0.06 ± 1.06	28.82 ± 0.09 ± 2.39	10.71 ± 0.05 ± 0.89	52.36 ± 0.12 ± 4.35
Drell-Yan	4.83 ± 0.52 ± 1.26	3.56 ± 0.43 ± 0.93	2.82 ± 0.37 ± 0.73	11.21 ± 0.77 ± 2.91
$t\bar{t}$	0.05 ± 0.01 ± 0.01	0.11 ± 0.01 ± 0.01	0.04 ± 0.01 ± 0.00	0.20 ± 0.01 ± 0.02
WZ + ZZ	3.62 ± 0.02 ± 0.36	0.93 ± 0.01 ± 0.09	3.39 ± 0.01 ± 0.34	7.93 ± 0.02 ± 0.79
Wγ	3.57 ± 0.12 ± 0.71	3.25 ± 0.10 ± 0.65	0.02 ± 0.01 ± 0.00	6.83 ± 0.16 ± 1.37
W+jets	2.96 ± 0.23 ± 0.71	6.69 ± 0.41 ± 1.98	1.33 ± 0.17 ± 0.53	10.99 ± 0.50 ± 3.20
Sum Bkg	15.03 ± 0.58 ± 1.65	14.54 ± 0.60 ± 2.28	7.60 ± 0.41 ± 0.97	37.16 ± 0.93 ± 4.61
Expected	28± 0.59 ± 1.96	43± 0.61 ± 3.31	18± 0.41 ± 1.31	90± 0.94 ± 6.33
Data	29	47	19	95

Fig. 4.18. Summary of the number of WW events observed by CDF at 1.96 TeV with an integrated luminosity of 825 pb^{-1}. CDF observes 95 WW candidate events with a background of about 37.

The WW cross section at the Tevatron is predicted to be about 12 pb. Fig. 4.18 is a summary of the number of WW events observed by CDF at 1.96 TeV with an integrated luminosity of 825 pb[-1]. CDF observes 95 WW candidate events with a background of about 37 which yields the cross section given in Table 4.2. Fig. 4.19 shows a comparison of the WW cross-section measurements with the NLO theory predictions. The data agree well with the NLO theory prediction. There are now enough WW events to begin to study the details of WW production at the Tevatron.
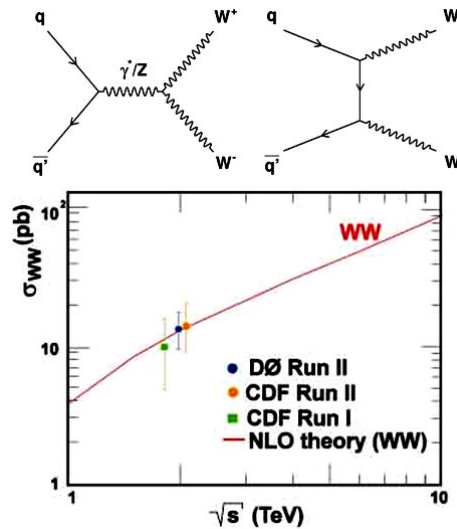

Fig. 4.19. (*top*) Leading order Feynman diagrams for W+W production at the Tevatron. (*bottom*) Comparison of Tevatron measurements for the cross section of W+W production with the NLO theory predictions.
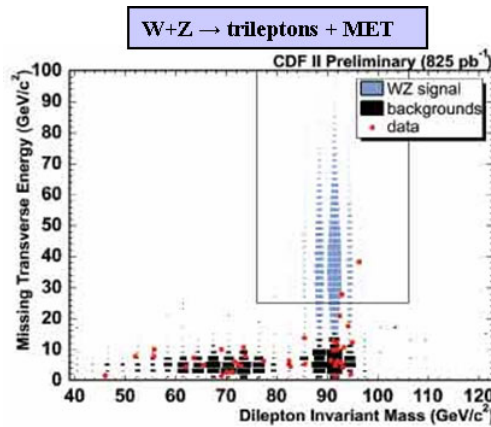

Fig. 4.20. CDF Run 2 search for W+Z production in proton-antiproton collisions at 1.96 TeV with an integrated luminosity of 825 pb[-1]. The signal corresponds to three leptons plus missing transverse energy (MET) and the plot shows the MET versus the invariant mass of the lepton-pairs. The signal region (rectangular box) shows 2 candidate events with a background of 0.9±0.2.

Fig. 4.20 shows the CDF search for W+Z events in a data sample with an integrated luminosity of 825 pb[-1]. They find 2 candidate events with a background of 0.9±0.2, which yields the upper limit shown in Table 4.2. We are very close to seeing W+Z production at the Tevatron.

Fig. 4.21 shows a summary of the boson and di-boson measurements at the Tevatron. The W cross section is around 26,000 pb. About a factor of 3 below the W cross section is the Z-boson cross section. About a factor of 40 below the Z-boson cross section are the W+γ and Z+γ cross sections. About a factor of 10 below the Z+γ cross section is the W+W cross section. About a factor of 3 below the W+W cross

section is the expected W+Z cross section which CDF and DØ will soon measure. At the Tevatron we have moved from measuring cross-sections at the 1,000 pb level to measuring cross-sections at the 1 pb level or smaller. The Higgs→WW cross section might be at the 0.1 pb level. We are getting close! Fig. 4.22 shows the errors on the top quark and W-boson mass at the 68% confidence level. Recent measurements favor a light Higgs mass of around 113 GeV. Also shown is the confidence level region expected with 8 fb⁻¹ of Tevatron data. A light Higgs mass is a very interesting scenario for the Tevatron.
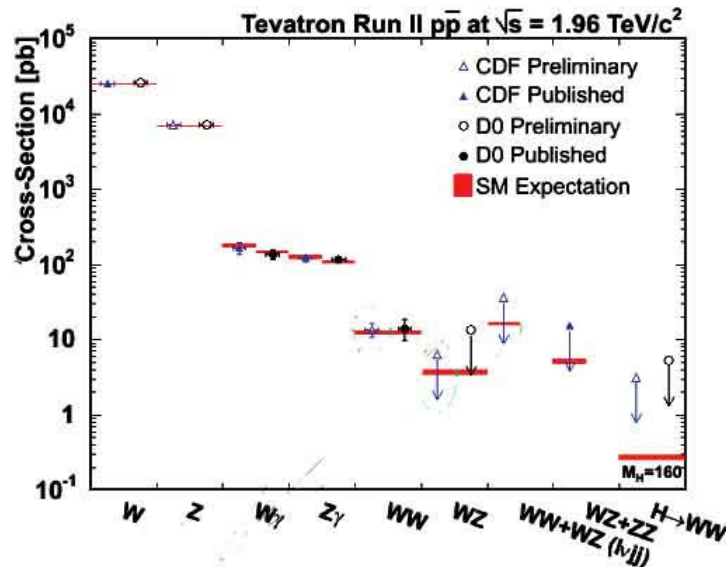
Fig. 4.21. Summary of the Tevatron measurements (or limits) of the cross sections for the production of W-bosons, Z-bosons, W+γ, Z+γ, W+W, W+Z, and Higgs→WW compared with the Standard Model predictions. CDF and DØ are beginning to measure cross-sections at the 1 pb level and are getting closer to the Higgs.

Fig. 4.22. Plot of the mass of the W-boson versus the top quark mass. The blue oval is the 68% confidence level region determined from the current LEP2 and Tevatron data. Recent data favor a light Higgs mass of around 113 GeV. The black circle is the 68% confidence level region expected with 8 fb⁻¹ of Tevatron data. A light Higgs mass is a very interesting scenario for the Tevatron.
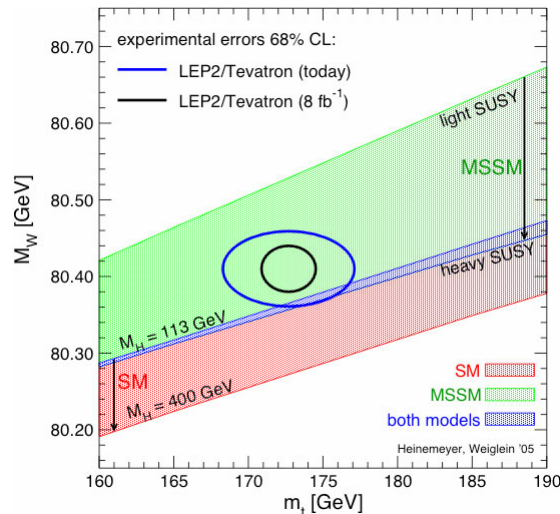
V. THE UNDERLYING EVENT AND MONTE-CARLO TUNES

In order to find "new" physics at a hadron-hadron collider it is essential to have Monte-Carlo models that simulate accurately the "ordinary" QCD hard-scattering events. To do this one must not only have a good model of the hard scattering part of the process, but also of the beam-beam remnants and the multiple parton interactions. The "underlying event" is an unavoidable background to most collider observables and a good understanding of it will lead to more precise measurements at the Tevatron and the LHC. We have seen that at the Tevatron both the inclusive jet cross section and the b-jet cross section are sensitively on the "underlying event". At CDF we are working to understand and model the "underlying event" at the Tevatron.

We are also trying to extrapolate what we are learning at the Tevatron to the LHC. We use the topological structure of hadron-hadron collisions to study the "underlying event" [25-27]. The direction of the leading calorimeter jet is used to isolate regions of η-ϕ space that are sensitive to the "underlying event". As illustrated in Fig. 5.1, the direction of the leading jet, jet#1, is used to define correlations in the azimuthal angle, $\Delta\phi$. The angle $\Delta\phi = \phi - \phi_{jet\#1}$ is the relative azimuthal angle between a charged particle and the direction of jet#1. The "transverse" region is almost perpendicular to the plane of the hard 2-to-2 scattering and is therefore very sensitive to the "underlying event". Furthermore, we consider two classes of events. We refer to events in which there are no restrictions placed on the second and third highest P_T jets (jet#2 and jet#3) as "leading jet" events. Events with at least two jets with $P_T > 15$ GeV where the leading two jets are nearly "back-to-back" ($|\Delta\phi_{12}| > 150^o$) with $P_T(jet\#2)/P_T(jet\#1) > 0.8$ and $P_T(jet\#3) < 15$ GeV are referred to as "back-to-back" events. "Back-to-back" events are a subset of the "leading jet" events. The idea here is to suppress hard initial and final-state radiation thus increasing the sensitivity of the "transverse" region to the "beam-beam remnant" and the multiple parton scattering component of the "underlying event".

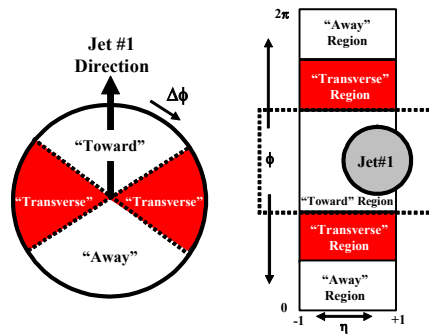**Fig. 5.1.** Illustration of correlations in azimuthal angle $\Delta\phi$ relative to the direction of the leading jet (MidPoint, R = 0.7, $f_{merge} = 0.75$) in the event, jet#1. The angle $\Delta\phi = \phi - \phi_{jet\#1}$ is the relative azimuthal angle between charged particles (or calorimeter towers) and the direction of jet#1. The "transverse" region is defined by $60^o < |\Delta\phi| < 120^o$ and $|\eta| < 1$. We examine charged particles in the range $p_T > 0.5$ GeV/c and $|\eta| < 1$, but allow the leading jet to be in the region $|\eta(jet\#1)| < 2$.

As illustrated in Fig. 5.2, we define a variety of MAX and MIN "transverse" regions which helps separate the "hard component" (initial and final-state radiation) from the "beam-beam remnant" component. MAX (MIN) refer to the "transverse" region containing the largest (smallest) number of charged particles or the region containing the largest (smallest) scalar p_T sum of particles. Since we will be studying
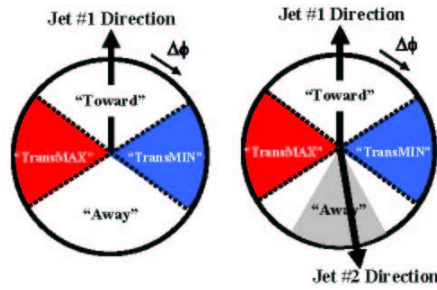
Fig. 5.2. Illustration of correlations in azimuthal angle $\Delta\phi$ relative to the direction of the leading jet (highest P_T jet) in the event, jet#1 for "leading jet" events (*left*) and "back-to-back" events (*right*). Events in which there are no restrictions placed on the on the second highest P_T jet, jet#2, are referred to as "leading jet" events. Events with at least two jets where the leading two jets are nearly "back-to-back" ($\Delta\phi_{12} > 150^o$) with P_T(jet#2)/P_T(jet#1) > 0.8 and P_T(jet#3) < 15 GeV/c are referred to as "back-to-back" events. In both cases the angle $\Delta\phi = \phi - \phi$jet#1 is the relative azimuthal angle between charged particles and the direction of jet#1. On an event by event basis, we define "transMAX" ("transMIN") to be the maximum (minimum) of the two "transverse" regions, $60^o < \Delta\phi < 120^o$ and $60^o < -\Delta\phi < 120^o$. "TransMAX" and "transMIN" each have an area in η-ϕ space of $\Delta\eta\Delta\phi = 4\pi/6$. The overall "transverse" region defined in Fig. 5.1 includes both the "transMAX" and the "transMIN" region.
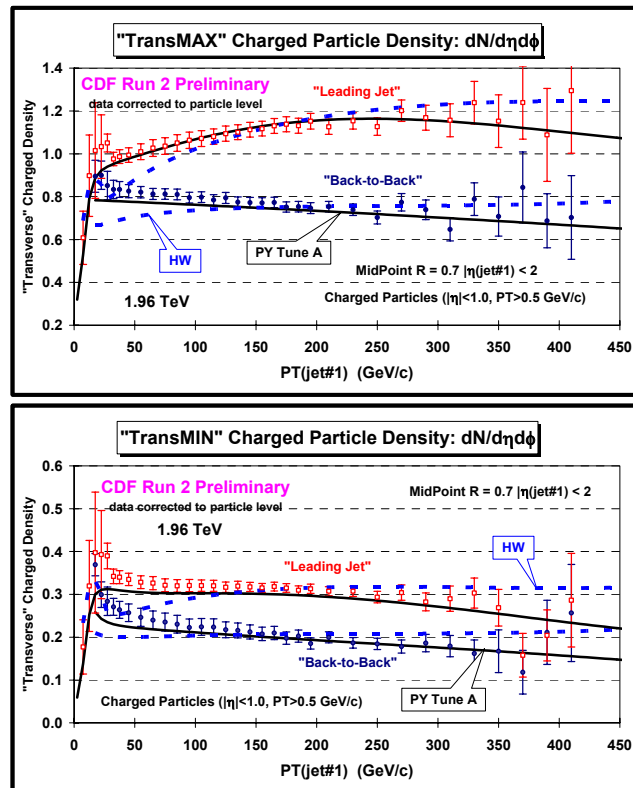

Fig. 5.3. CDF Run 2 data at 1.96 TeV on charged particle density, dN/dηdϕ, with $p_T > 0.5$ GeV/c and $|\eta| < 1$ in the "transMAX" region (*top*) and the "transMIN" region (*bottom*) for "leading jet" and "back-to-back" events as defined in Fig. 5.2 as a function of the leading jet P_T compared with PYTHIA Tune A and HERWIG. The data are corrected to the particle level (with errors that include both the statistical error and the systematic uncertainty) and compared with the theory at the particle level (*i.e.* generator level).

regions in η-ϕ space with different areas, we construct densities by dividing by the area. For example, the charged particle density, dN/dηdϕ, corresponds number of charged particle with $p_T > 0.5$ GeV/c per unit η-ϕ, and the PTsum density, dPTsum/dηdϕ, corresponds the amount of charged particle ($p_T > 0.5$ GeV/c) scalar p_T sum per unit η-ϕ. The overall "transverse" region defined in Fig. 5.1 includes both the "transMAX" and the "transMIN" region. One expects that "transMAX" will pick

up the hardest initial or final-state radiation while both "transMAX" and "transMIN" should receive "beam-beam remnant" contributions. Hence one expects "transMIN" to be more sensitive to the "beam-beam remnant" component of the "underlying event", while the "transMAX" minus the "transMIN" (*i.e.* "transDIF") is very sensitive to initial and final-state radiation. This idea, was first suggested by Bryan Webber, and implemented by in a paper by Jon Pumplin [28]. Also, Valaria Tano studied this in her CDF Run 1 analysis of maximum and minimum transverse cones [29].
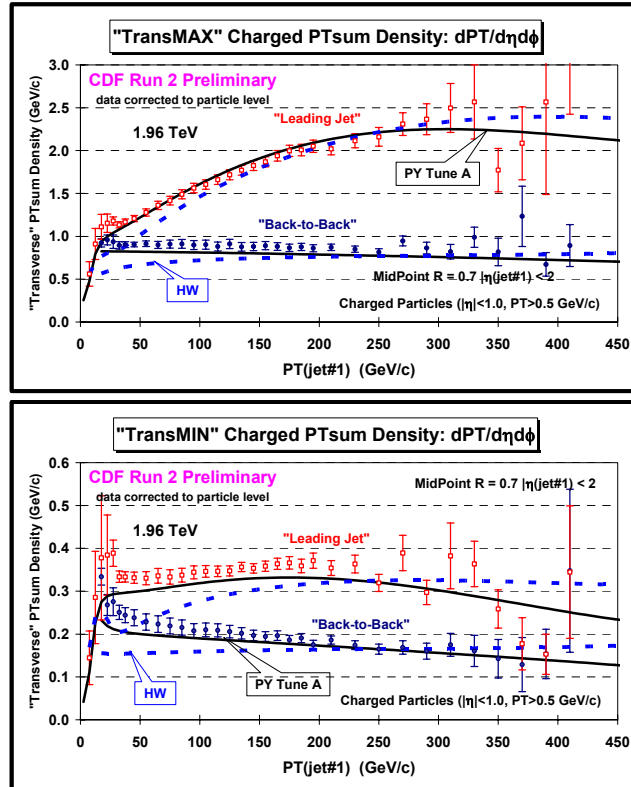

Fig. 5.4. CDF Run 2 data at 1.96 TeV on scalar PTsum density of charged particles, dPT/dηdφ, with $p_T > 0.5$ GeV/c and $|\eta| < 1$ in the "transMAX" region (*top*) and the "transMIN" region (*bottom*) for "leading jet" and "back-to-back" events as defined in Fig. 5.2 as a function of the leading jet P_T compared with PYTHIA Tune A and HERWIG. The data are corrected to the particle level (with errors that include both the statistical error and the systematic uncertainty) and compared with the theory at the particle level (*i.e.* generator level).

Fig. 5.3 and Fig. 5.4 show the CDF Run 2 data on the density of charged particles and the charged PTsum density in the "transMAX" and "transMIN" regions for "leading jet" and "back-to-back" events. The data are compared with PYTHIA Tune A (with multiple parton interactions) and HERWIG (without multiple parton interactions). PYTHIA Tune A was determined by fitting the CDF Run 1 "underlying event" data [25].

As expected, the "leading jet" and "back-to-back" events behave quite differently. For the "leading jet" case the "transMAX" densities rise with increasing P_T(jet#1), while for the "back-to-back" case they fall with increasing P_T(jet#1). The rise in the "leading jet" case is, of course, due to hard initial and final-state radiation, which has been suppressed in the "back-to-back" events. The "back-to-back" events allow for a closer look at the "beam-beam remnant" and multiple parton scattering component of

the "underlying event" and PYTHIA Tune A does a better job describing the data than HERWIG.

The "transMIN" densities are more sensitive to the "beam-beam remnant" and multiple parton interaction component of the "underlying event". The "back-to-back" data show a decrease in the "transMIN" densities with increasing P_T(jet#1) which is described fairly well by PYTHIA Tune A but not by HERWIG. The decrease of the "transMIN" densities with increasing P_T(jet#1) for the "back-to-back" events is very interesting and might be due to a "saturation" of the multiple parton interactions at small impact parameter. Such an effect is included in PYTHIA Tune A but not in HERWIG (without multiple parton interactions).
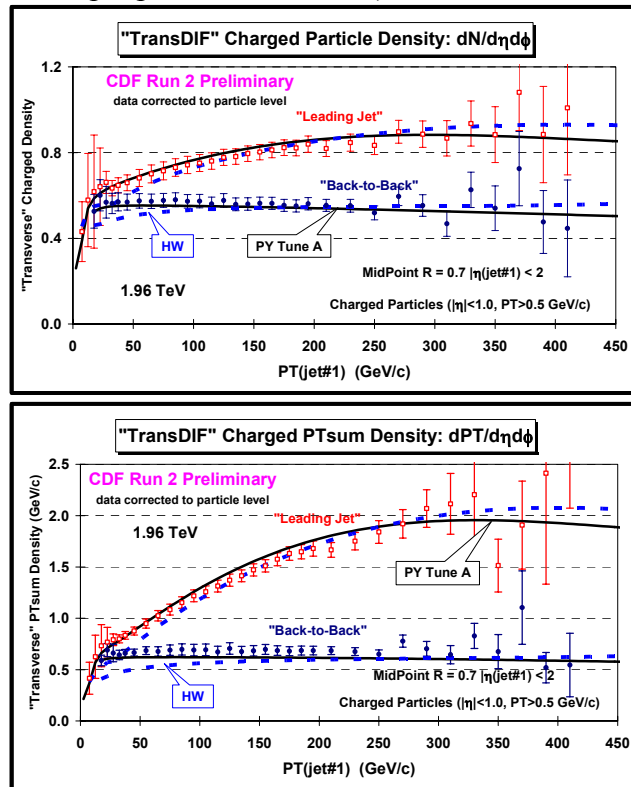

Fig. 5.5. CDF Run 2 data at 1.96 TeV on the density of charged particles, dN/dηdϕ (*top*), and the charged PTsum density, dPT/dηdϕ (*bottom*), with $p_T > 0.5$ GeV/c and $|\eta| < 1$ for "transMAX" minus "transMIN" for "leading jet" and "back-to-back" events as defined in Fig. 5.2 as a function of the leading jet P_T compared with PYTHIA Tune A and HERWIG. The data are corrected to the particle level (with errors that include both the statistical error and the systematic uncertainty) and compared with the theory at the particle level (*i.e.* generator level).

Fig. 5.5 and Fig. 5.6 compares the CDF Run 2 data on the density of charged particles and the charged PTsum density for "transDIF" and for the overall "transverse" region, respectively, with PYTHIA Tune A and HERWIG for "leading jet" and "back-to-back" events. The average p_T for charged particles with with $p_T > 0.5$ GeV/c and $|\eta| < 1$ in the overall "transverse" region for "leading jet" and "back-to-back" events are compared with PYTHIA Tune A and HERWIG in Fig. 5.7. Both PYTHIA Tune A and HERWIG lie below the data, but PYTHIA Tune A does a much better job that HERWIG. HERWIG (without multiple parton interactions) predicts a "softer" p_T distribution of charged particles than is seen in the data.
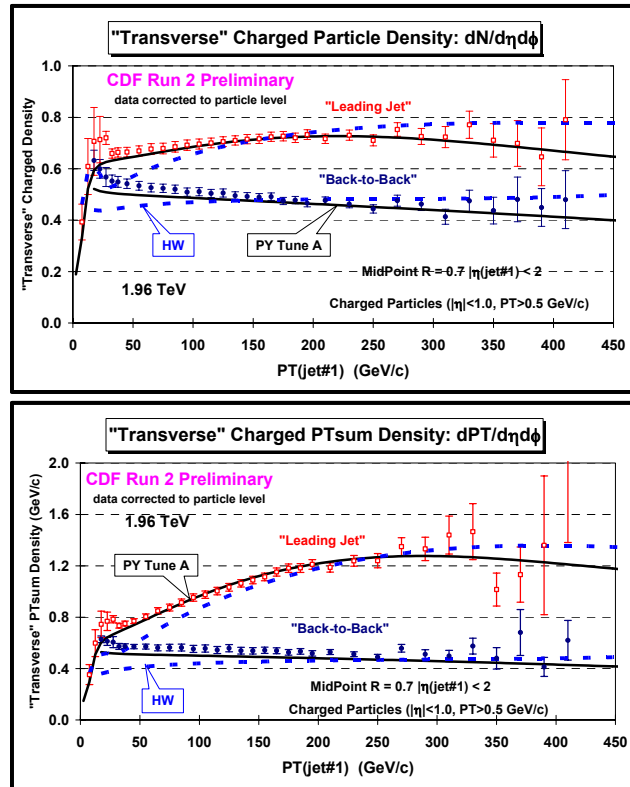
Fig. 5.6. CDF Run 2 data at 1.96 TeV on the density of charged particles, $dN/d\eta d\phi$ (*top*), and the charged PTsum density, $dPT/d\eta d\phi$ (*bottom*), with $p_T > 0.5$ GeV/c and $|\eta| < 1$ in the avarall "transverse" region (average of "transMAX" and "transMIN") for "leading jet" and "back-to-back" events as defined in Fig. 5.2 as a function of the leading jet P_T compared with PYTHIA Tune A and HERWIG. The data are corrected to the particle level (with errors that include both the statistical error and the systematic uncertainty) and compared with the theory at the particle level (*i.e.* generator level).

Fig. 5.7. CDF Run 2 data at 1.96 TeV average p_T of charged particles with $p_T > 0.5$ GeV/c and $|\eta| < 1$ in the overall "transverse" region for "leading jet" and "back-to-back" events as defined in Fig. 5.2 as a function of the leading jet P_T compared with PYTHIA Tune A and HERWIG. The data are corrected to the particle level (with errors that include both the statistical error and the systematic uncertainty) and compared with the theory at the particle level (*i.e.* generator level).
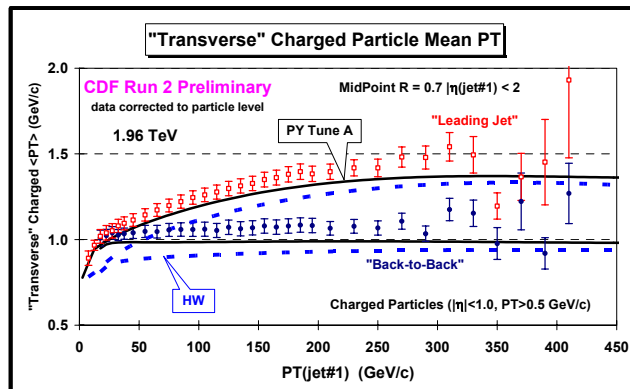
As illustrated in Fig. 5.8, Drell-Yan lepton-pair production provides an excellent place to study the underlying event. Here one studies the outgoing charged particles (excluding the lepton pair) as a function of the lepton-pair invariant mass. After removing the lepton-pair everything else results from the beam-beam remnants,

multiple parton interactions, and initial-state radiation. Unlike high p_T jet production (Fig. 2.8) for lepton-pair production there is no final-state gluon radiation.
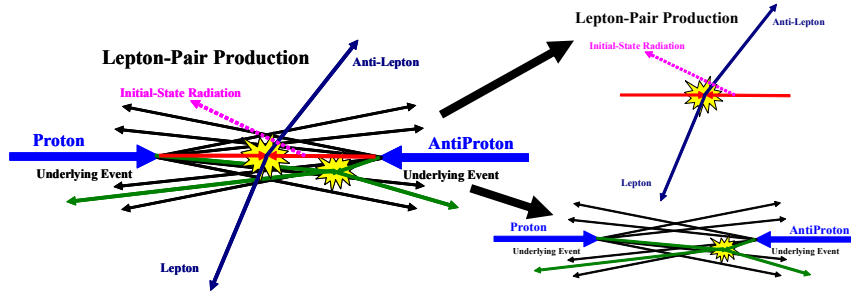
Fig. 5.8. Illustration of the way QCD Monte-Carlo models simulate Drell-Yan lepton-pair production. The "hard scattering" component of the event consists of the two outgoing leptons plus particles that result from initial-state radiation. The "underlying event" consists of particles that arise from the "beam-beam remnants" and from multiple parton interactions.

Fig. 5.10. CDF Run 1 data on the Z-boson p_T distribution compared with PYTHIA Tune A, Tune AW, Tune DW, and HERWIG.

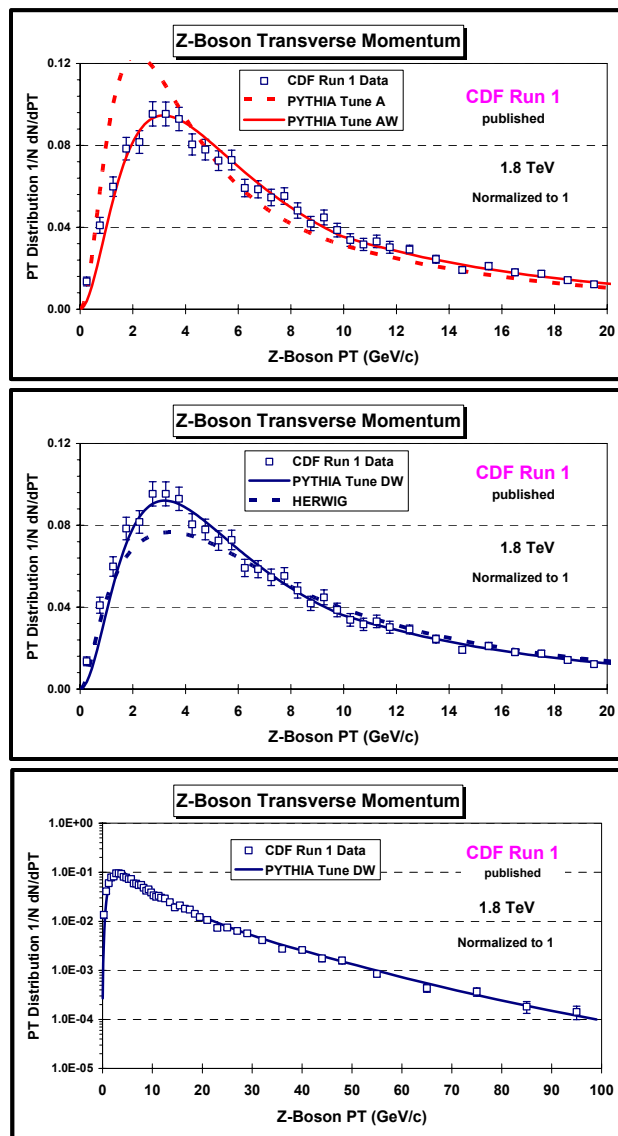Fig. 5.10 shows that PYTHIA Tune A does not fit the CDF Run 1 Z-boson p_T distribution [30]. PYTHIA Tune A was determined by fitting the Run 1 "underlying event" data and, at that time, we did not consider the Z-boson data. PYTHIA Tune AW fits the Z-boson p_T distribution as well as the "underlying event" at the Tevatron [31]. PYTHIA TuneAW is compared with the CDF Run 2 Z-boson p_T distribution in Fig. 4.6. HERWIG does a fairly good job fitting the Z-boson p_T distribution without additional tuning, but does not fit the CDF "underlying event" data.
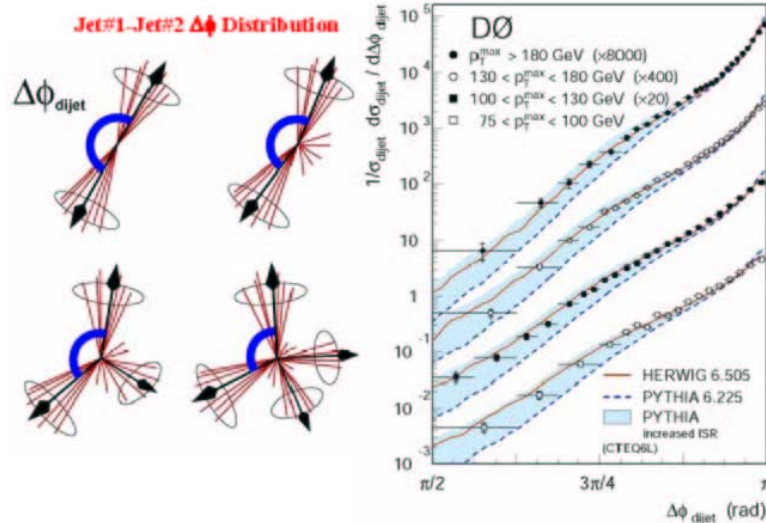

Fig. 5.11. Shows the DØ Run 2 jet#1-jet#2 $\Delta\phi$ distribution at 1.96 TeV compared with PYTHIA (*default*) and PYTHIA Tune A (upper edge of the shaded regions). Jet#1 and jet#2 are the leading two jets (MidPoint algorithm, R = 0.7, f_{merge} = 0.5). The best PYTHIA fit to this data is with PARP(67) = 2.5.

Table 5.1. Parameters for several PYTHIA 6.2 tunes. Tune A is a CDF Run 1 "underlying event" tune. Tune AW, DW, DWT, and BW are CDF Run 2 tunes which fit the existing Run 2 "underlying event" data and fit the Run 1 Z-boson p_T distribution. Tune QW is vary similar to Tune DW except that it uses the next-to-leading order structure function CTEQ6.1. The ATLAS Tune is the default tune currently used by ATLAS at the LHC. The first 9 parameters tune the multiple parton interactions. PARP(62), PARP(62), and PARP(62) tune the initial-state radiation and the last three parameters set the intrensic k_T of the partons within the incoming proton and antiproton.

Parameter	Tune A	Tune AW	Tune DW	Tune DWT	Tune BW	ATLAS	Tune QW
PDF	CTEQ5L	CTEQ5L	CTEQ5L	CTEQ5L	CTEQ5L	CTEQ5L	CTEQ6.1
MSTP(81)	1	1	1	1	1	1	1
MSTP(82)	4	4	4	4	4	4	4
PARP(82)	2.0	2.0	1.9	1.9409	1.8	1.8	1.1
PARP(83)	0.5	0.5	0.5	0.5	0.5	0.5	0.5
PARP(84)	0.4	0.4	0.4	0.4	0.4	0.5	0.4
PARP(85)	0.9	0.9	1.0	1.0	1.0	0.33	1.0
PARP(86)	0.95	0.95	1.0	1.0	1.0	0.66	1.0
PARP(89)	1800	1800	1800	1960	1800	1000	1800
PARP(90)	0.25	0.25	0.25	0.16	0.25	0.16	0.25
PARP(62)	1.0	1.25	1.25	1.25	1.25	1.0	1.25
PARP(64)	1.0	0.2	0.2	0.2	0.2	1.0	0.2
PARP(67)	4.0	4.0	2.5	2.5	1.0	1.0	2.5
MSTP(91)	1	1	1	1	1	1	1
PARP(91)	1.0	2.1	2.1	2.1	2.1	1.0	2.1
PARP(93)	5.0	15.0	15.0	15.0	15.0	5.0	15.0

Table 5.1 shows the parameters for several PYTHIA 6.2 tunes. PYTHIA Tune DW is very similar to Tune AW except PARP(67) = 2.5, which is the preferred value determined by DØ in fitting their dijet $\Delta\phi$ distribution shown in Fig. 5.11 [32]. PARP(67) sets the high p_T scale for initial-state radiation in PYTHIA. It determines the maximal parton virtuality allowed in time-like showers. Tune BW is a tune with PARP(67) = 1.0. Tune DW and Tune DWT are identical at 1.96 TeV, but Tune DW and DWT extrapolate differently to the LHC. Tune DWT uses the ATLAS energy dependence, PARP(90) = 0.16, while Tune DW uses the Tune A value of PARP(90) = 0.25. The ATLAS Tune is the default tune currently used by ATLAS at the LHC. All the tunes except Tune QW use CTEQ5L.

The first 9 parameters in Table 5.1 tune the multiple parton interactions (MPI). PARP(62), PARP(64), and PARP(67) tune the initial-state radiation and the last three parameters set the intrinsic k_T of the partons within the incoming proton and antiproton.

Table 5.2. Shows the computed value of the multiple parton scattering cross section for the various PYTHIA 6.2 tunes.

Tune	σ(MPI) at 1.96 TeV	σ(MPI) at 14 TeV
A, AW	309.7 mb	484.0 mb
DW	351.7 mb	549.2 mb
DWT	351.7 mb	829.1 mb
BW	401.7 mb	624.8 mb
QW	296.5 mb	568.7 mb
ATLAS	324.5 mb	768.0 mb

Tune QW uses CTEQ6.1 which is a next-to-leading order structure function. However, Tune QW uses leading order QCD coupling, α_s, with Λ = 0.192 GeV. Note that Tune QW has a much smaller value of PARP(82) (*i.e.* the MPI cut-off). This is due to the change in the low x gluon distribution in going from CTEQ5L to CTEQ6.1. Table 5.2 shows the computed value of the multiple parton scattering cross section for the various tunes. The multiple parton scattering cross section (divided by the total inelastic cross section) determines the average number of multiple parton collisions per event.

As can be seen in Figs. 5.11 – 5.13, PYTHIA Tune A, AW, DW, DW, and QW have been adjusted to give similar results for the charged particle density and the PTsum density in the "transverse" region with p_T > 0.5 GeV/c and $|\eta|$ < 1 for "leading jet" events at 1.96 TeV. PHYTIA Tune A agrees fairly well with the CDF Run 2 "underlying event" data for "leading jet" events and Tune AW, BW, DW, and QW roughly agree with Tune A. Fig. 5.12 shows that PYTHIA Tune A, Tune DW, and the ATLAS PYTHIA Tune predict about the same density of charged particles in the "transverse" region with p_T > 0.5 GeV/c for "leading jet" events at the Tevatron. However, the ATLAS Tune has a much softer p_T distribution of charged particles resulting in a much smaller average p_T per particles. Fig. 5.14 shows that the softer p_T distribution of the ATLAS Tune does not agree with the CDF data from Fig. 5.7.
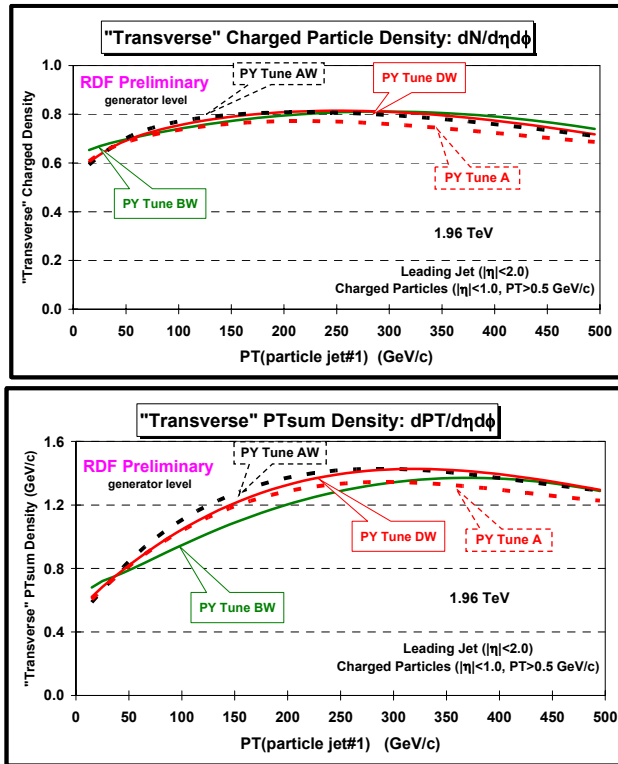
Fig. 5.11. Predictions at 1.96 TeV of PYTHIA Tune A, Tune AW, Tune BW, and Tune DW for the density of charged particles, dN/dηdφ (*top*), and the charged PTsum density, dPT/dηdφ (*bottom*), with p_T > 0.5 GeV/c and |η| < 1 in the overall "transverse" region for "leading jet" events as defined in Fig. 5.2 as a function of the leading jet P_T.

Fig. 5.12. Predictions at 1.96 TeV of PYTHIA Tune DW (DWT), HERWIG, and the ATLAS Tune for the density of charged particles, dN/dηdφ (*top*), and the charged PTsum density, dPT/dηdφ (*bottom*), with p_T > 0.5 GeV/c and

$|\eta| < 1$ in the overall "transverse" region for "leading jet" events as defined in Fig. 5.2 as a function of the leading jet P_T. Tune DW and DWT are identical at 1.96 TeV.
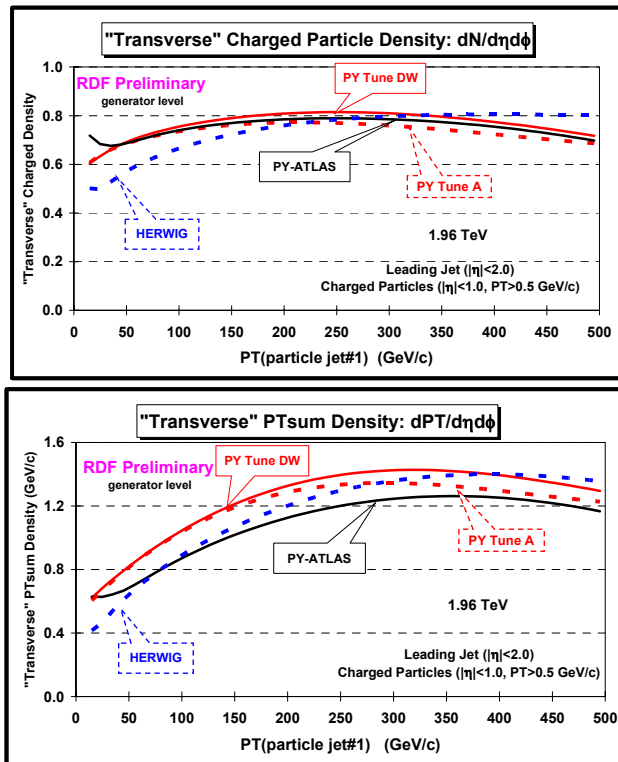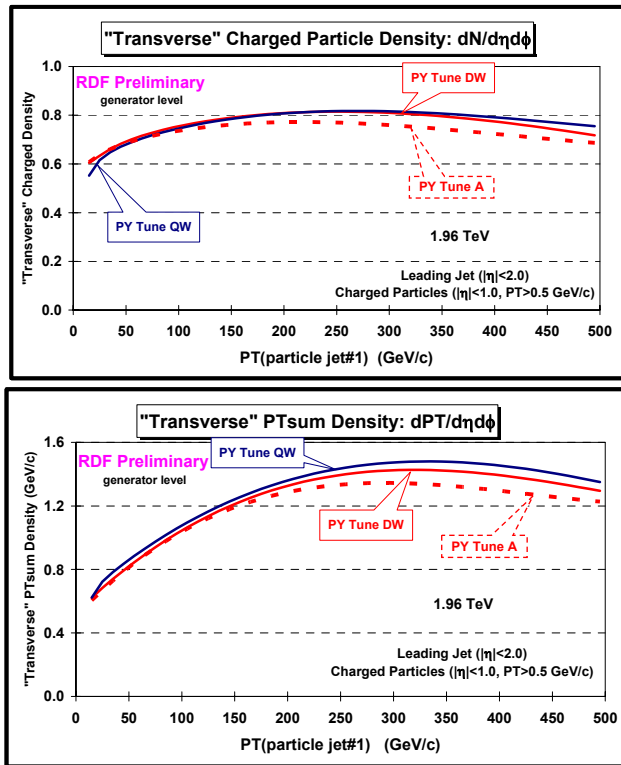

Fig. 5.13. Predictions at 1.96 TeV of PYTHIA Tune A, Tune DW, and Tune QW for the density of charged particles, dN/dηdφ (*top*), and the charged PTsum density, dPT/dηdφ (*bottom*), with $p_T > 0.5$ GeV/c and $|\eta| < 1$ in the overall "transverse" region for "leading jet" events as defined in Fig. 5.2 as a function of the leading jet P_T.
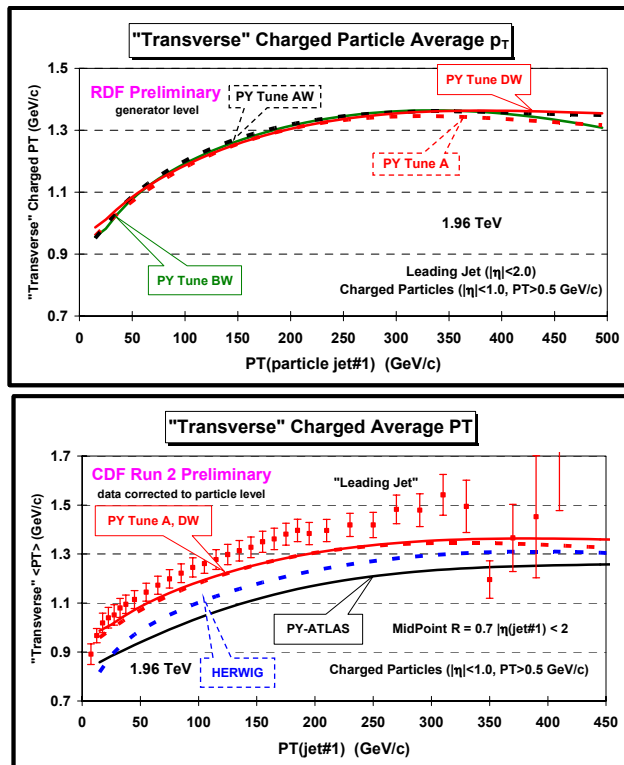

Fig. 5.14. (*top*) Predictions of PYTHIA Tune A, Tune AW, Tune BW, and Tune DW for average p_T of charged particles with $p_T > 0.5$ GeV/c and $|\eta| < 1$ in the overall "transverse" region for "leading jet" events at 1.96 TeV as a

function of the leading jet P_T. (*bottom*) CDF Run 2 data at 1.96 TeV on the average p_T of charged particles with p_T > 0.5 GeV/c and $|\eta|$ < 1 in the overall "transverse" region for "leading jet" events as a function of the leading jet P_T compared with PYTHIA Tune A, Tune DW, HERWIG, and the ATLAS PYTHIA Tune.
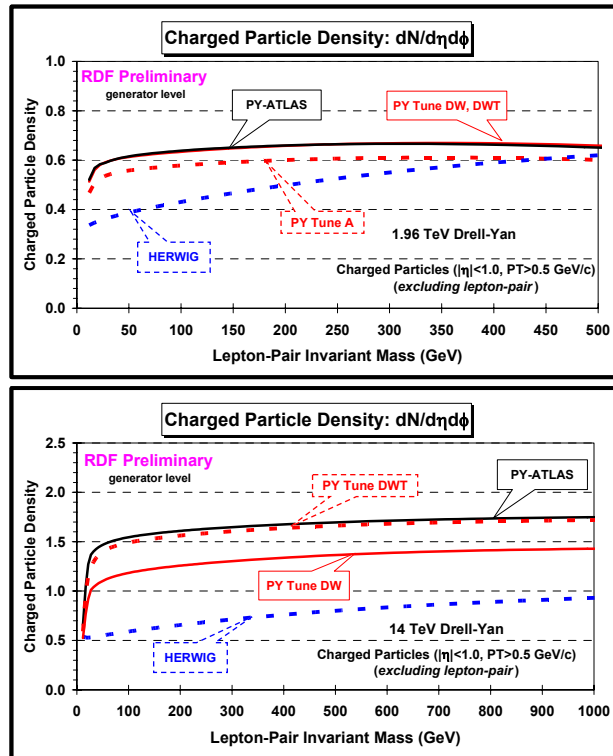

Fig. 5.15. Predictions of PYTHIA Tune A, Tune DW, Tune DWT, HERWIG, and the ATLAS PYTHIA Tune for the density of charged particles, dN/dηdφ, with p_T > 0.5 GeV/c and $|\eta|$ < 1 in Drell-Yan lepton-pair production (excluding the lepton-pair) at 1.96 TeV (*top*) and 14 TeV (*bottom*) as a function of the invariant mass of the lepton pair. Tune DW and Tune DWT are identical at 1.96 TeV.
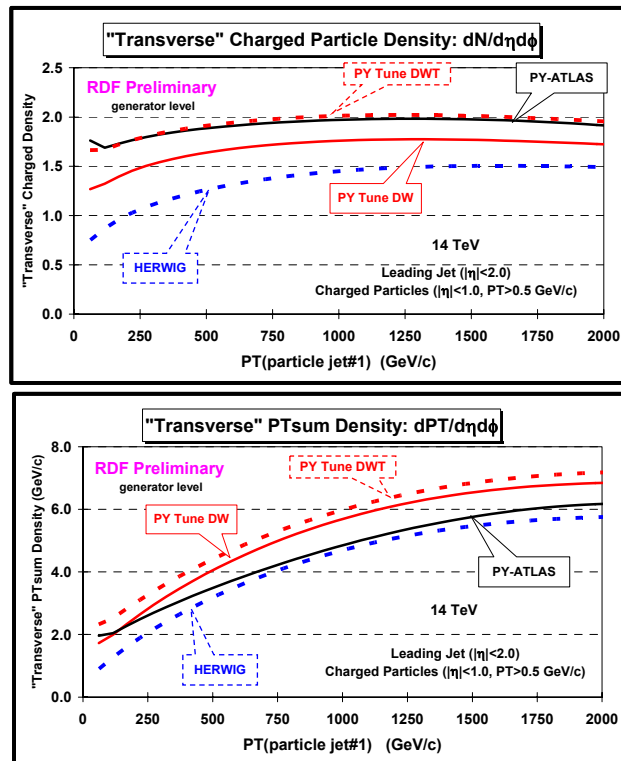
Fig. 5.16. Predictions at 14 TeV of PYTHIA Tune DW, Tune DWT, HERWIG, and the ATLAS Tune for the density of charged particles, $dN/d\eta d\phi$ (*top*), and the charged PTsum density, $dPT/d\eta d\phi$ (*bottom*), with $p_T > 0.5$ GeV/c and $|\eta| < 1$ in the overall "transverse" region for "leading jet" events as a function of the leading jet P_T.

The predictions of PYTHIA Tune A, Tune DW, Tune DWT, HERWIG, and the ATLAS PYTHIA Tune for the density of charged particles with $p_T > 0.5$ GeV/c and $|\eta| < 1$ for Drell-Yan lepton-pair production at 1.96 TeV and 14 TeV are shown in Fig. 5.15. The ATLAS Tune and Tune DW predict about the same charged particle density with $p_T > 0.5$ GeV/c at the Tevatron, and the ATLAS Tune and Tune DWT predict about the same charged particle density with $p_T > 0.5$ GeV/c at the LHC. However, the ATLAS Tune has a much softer p_T distribution of particles, both at the Tevatron and the LHC. We are working to compare the CDF Run 2 data on Drell-Yan production with the QCD Monte-Carlo models and hope to have results soon.

Fig. 5.16 shows the predictions of PYTHIA Tune DW, Tune DWT, HERWIG, and the ATLAS Tune for the density of charged particles and the PTsum density in the "transverse" region for "leading jet" production at the LHC. The PYTHIA Tunes (with multiple parton interactions) predict a large increase in the charged particle density in going from the Tevatron (Fig. 5.12) to the LHC (Fig. 5.16). HERWIG (without multiple parton interactions) does not increase as much. At the LHC PYTHIA Tune DWT and the ATLAS Tune both predict about the same charged particle density with $p_T > 0.5$ GeV/c, however, the ATLAS Tune predicts a smaller PTsum density than Tune DWT (*i.e.* the ATLAS Tune produces a softer p_T distribution here as well).
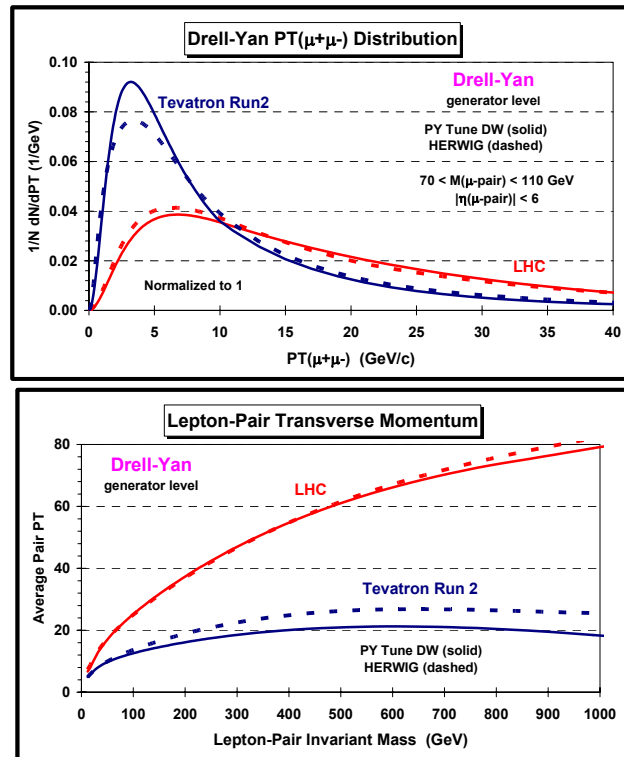

Fig. 5.17. Predictions at 1.96 TeV (Tevatron Run 2) and 14 TeV (LHC) of PYTHIA Tune DW and HERWIG for (*top*) the lepton-pair p_T distribution at the Z-boson mass and (*bottom*) the average lepton-pair p_T versus the lepton pair invariant mass.

The increased amount of initial-state radiation at the LHC results in a broader lepton-pair p_T distribution compared to the Tevatron. As can be seen in Fig. 5.17, even at the Z-boson mass the lepton-pair p_T distribution is predicted to be much broader at the LHC. This is indirectly related to the underlying event. More initial-state radiation results in a more active underlying event.
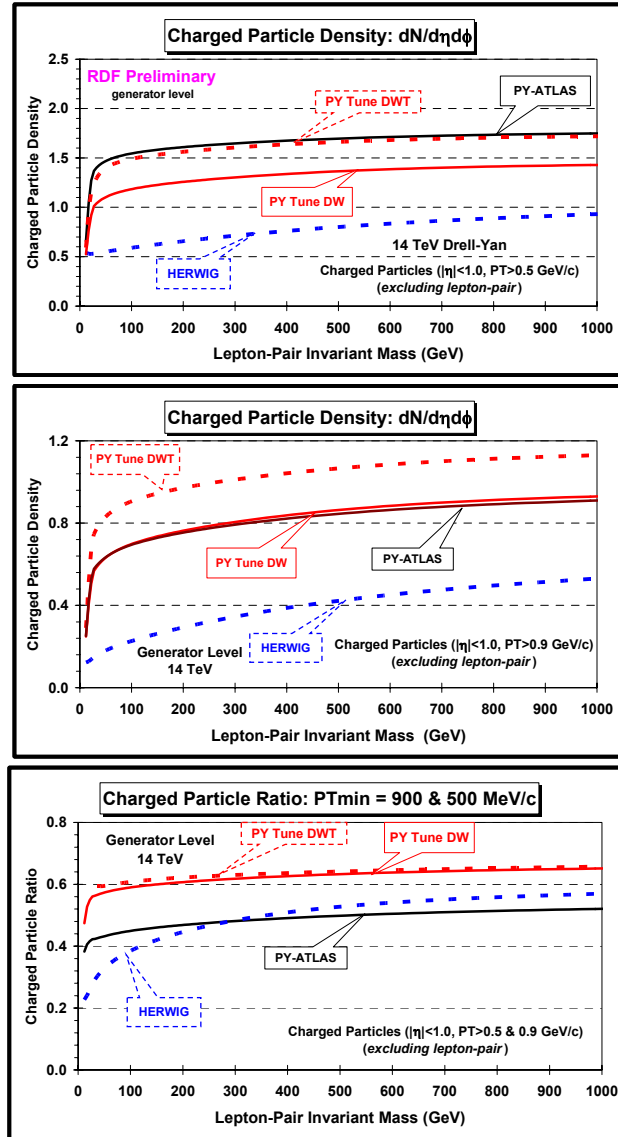

Fig. 5.18. Predictions at 14 TeV of PYTHIA Tune DW, Tune DWT, HERWIG, and the ATLAS Tune for the density of charged particles, dN/dηdφ, with |η| < 1 and p_T > 0.5 GeV/c (*top*) and p_T > 0.9 GeV/c (*middle*) for Drell-Yan lepton-pair production (excluding the lepton-pair) as a function of the lepton-pair invariant mass. (*bottom*) The ratio of the charged particle density with p_T > 0.9 GeV/c and p_T > 0.5 GeV/c.

Fig. 5.18 shows the predictions at 14 TeV of PYTHIA Tune DW, Tune DWT, HERWIG, and the ATLAS Tune for the density of charged particles with |η| < 1 and p_T > 0.5 GeV/c and p_T > 0.9 GeV/c for Drell-Yan lepton-pair production (excluding the lepton-pair) as a function of the lepton-pair invariant mass. The ratio of the two p_T thresholds clearly shows that the ATLAS tune has a much softer p_T distribution than the CDF tunes. We do not know what to expect at the LHC. I prefer PYTHIA Tune

DW or Tune DWT over the ATLAS Tune because these tunes fit the CDF Run 2 data much better than the ATLAS Tune.

We do not know what we will see at the LHC. Clearly the "underlying event" will be one of the first measurements and we may have to re-tune the QCD Monte-Carlo models at that time. In my opinion the best PYTHIA 6.2 tune at present is Tune DW or DWT. These tunes are identical at the 1.96 TeV and they do a good job fitting the CDF Run 2 "underlying event" data. I expect they will do a good job in describing the underlying event in Drell-Yan lepton-pair production at the Tevatron (but we will have to wait for the data). More work will have to be done in studying the "universality" of these tunes. For example, we do not know if Tune DW will correctly describe the underlying event in top quark production. Tune QW (or the corresponding Tune QWT) is vary similar to Tune DW (or Tune DWT) except that it uses the next-to-leading order structure function CTEQ6.1. Many Monte-Carlo based analyses use the 40 error PDF's associated with CTEQ6.1 and it is useful to have a tune using the central fit (*i.e.* CTEQ6.1).

ACKNOWLEDGEMENTS

REFERENCES

1. (FF1) *Quark Elastic Scattering as a Source of High Transverse Momentum Mesons*, R. D. Field and R. P. Feynman, Phys. Rev. **D15**, 2590-2616 (1977).
2. (FFF1) *Correlations Among Particles and Jets Produced with Large Transverse Momenta*, R. P. Feynman, R. D. Field and G. C. Fox, Nucl. Phys. **B128**, 1-65 (1977).
3. *Can Existing High Transverse Momentum Hadron Experiments be Interpreted by Contemporary Quantum Chromodynamics Ideas?*, R. D. Field, Phys. Rev. Letters **40**, 997-1000 (1978).
4. (FFF2) *A Quantum Chromodynamic Approach for the Large Transverse Momentum Production of Particles and Jets*, R. P. Feynman, R. D. Field and G. C. Fox, Phys. Rev. **D18**, 3320-3343 (1978).
5. (FF2) *A Parameterization of the properties of Quark Jets*, R. D. Field and R. P. Feynman, Nucl. Phys. **B136**, 1-76 (1978).
6. (FW1) *A QCD Model for e^+e^- Annihilation*, R. D. Field and S. Wolfram, Nucl. Phys. **B213**, 65-84 (1983).
7. F. Paige and S. Protopopescu, BNL Report, BNL38034, 1986 (unpublished), version 7.32.
8. G. Marchesini and B. R. Webber, Nucl. Phys **B310**, 461 (1988); I. G. Knowles, Nucl. Phys. **B310**, 571 (1988); S. Catani, G. Marchesini, and B. R. Webber, Nucl. Phys. **B349**, 635 (1991).
9. T. Sjostrand, Phys. Lett. **157B**, 321 (1985); M. Bengtsson, T. Sjostrand, and M. van Zijl, Z. Phys. **C32**, 67 (1986); T. Sjostrand and M. van Zijl, Phys. Rev. **D36**, 2019 (1987).
10. B. Andersson, G. Gustafson, G. Ingelman, and T. Sjostrand, Phys. Rep. **97**, 31 (1983).
11. Yu. Dokshitzer, S. Troyan, XiX Winter School of LNPI, vol 1, 144 (1984); A.H. Mueller, Nucl. Phys. **B213**, 85 (1983).
12. Ya. I. Azimov, Yu. Dokshitzer, V. Khoze, S. Troyan, Z. Phys. **C27**, 65 (1985).
13. S. D. Ellis and D.E. Soper, Phys. Rev. **D18**, 3160 (1993).
14. M. Cacciari and P. Nason, JHEP 0309:006 (2003).
15. *The Sources of b-Quarks at the Tevatron and Their Correlations*, R. Field, Phys. Rev. **D65**, 094006, (2002).
16. M. Cacciari, S. Frixione, M.L. Mangano, P. Nason, and G. Ridolfi, JHEP 0407:033 (2004).

17. *The MC and NLO 3.1 Event Generator*, Stefano Frixione and Bryan R. Webber, CAVENDISH-HEP-05-09, hep-ph/0506182 (2005). *Matching NLO QCD and Parton Showers in Heavy Flavor Production*, Stefano Frixione, Paolo Nason, and Bryan R. Webber, JHEP 0308:007 (2003).

18. J.M. Butterworth, J.R. Forshaw, and M.H. Seymour, Z. Phys. **C7**, 637-646 (1996).

19. *Measurements of Bottom Anti-Botootm Azimuthal Production Correlations in Proton-Antiproton Collisions at 1.8 TeV*, CDF Collaboration (D. Acosta et al.), Phys. Rev. **D71**, 092001 (2005).

20. R. Bonciani, S. Catani, M.L. Mangano, P. Nason Nucl. Phys. **B529**, 424-450,1998; N. Kidonakis, R. Vogt, Phys. Rev. **D68**, 114014 (2003).

21. B.W. Harris, E. Laenen, L. Phaf, Z. Sullivan, and S. Weinzierl. Phys. Rev. **D66**, 054024 (2002); Z. Sullivan, Phys. Rev. **D70**, 114012 (2004); T. Tait, Phys. Rev. **D61**, 034001 (2000); A. Belyaev and E. Boos, Phys. Rev. **D63**, 034012 (2001).

22. Phys. Rev. **D65**, 112003 (2002).

23. R. Hamberg, W.L. van Neerven, T. Matsuura, Nucl. Phys. **B359**, 343-405 (1991), Erratum-ibid. **B644**, 403-404 (2002); R. Harlander and W. Kilgore, Phys. Rev. Lett. **88**, 201801 (2002).

24. J.M. Campbell and R.K. Ellis, Phys. Rev. **D60**, 113006 (1999).

25. *Charged Jet Evolution and the Underlying Event in Proton-Antiproton Collisions at 1.8 TeV*, The CDF Collaboration (T. Affolder et al.), Phys. Rev. **D65**, 092002 (2002).

26. *The Underlying Event in Large Transverse Momentum Charged Jet and Z-boson Production at 1.8 TeV*, talk presented by Rick Field at DPF2000, Columbus, OH, August 11, 2000.

27. *A Comparison of the Underlying Event in Jet and Min-Bias Events*, talk presented by Joey Huston at DPF2000, Columbus, OH, August 11, 2000. *The Underlying Event in Jet and Minimum Bias Events at the Tevatron*, talk presented by Valeria Tano at ISMD2001, Datong, China, September 1-7, 2001.

28. *Hard Underlying Event Corrections to Inclusive Jet Cross-Sections*, Jon Pumplin, Phys. Rev. **D57**, 5787 (1998).

29. *The Underlying Event in Hard Interactions at the Tevatron Proton-Antiproton Collider*, CDF Collaboration (D. Acosta et al.), Phys. Rev. **D70**, 072002 (2004).

30. *Measurement of the Z P_T Distribution in proton-Antiproton Collisionsat 1.8 TeV*, The CDF Collaboration (F. Abe et al.), Phys. Rev. Lett. **67**, 2937-2941 (1991).

31. The value of PARP(62), PARP(64), and PARP(91) was determined by CDF Electroweak Group. The "W" in Tune AW, BW, DW, DWT, QW stands for "Willis". I combined the "Willis" tune with Tune A, etc..

32. Phys. Rev. Lett. **94,** 221801 (2005).